Article

Cell Reports

A TLR3-Specific Adjuvant Relieves Innate Resistance to PD-L1 Blockade without Cytokine Toxicity in Tumor Vaccine Immunotherapy

Graphical Abstract

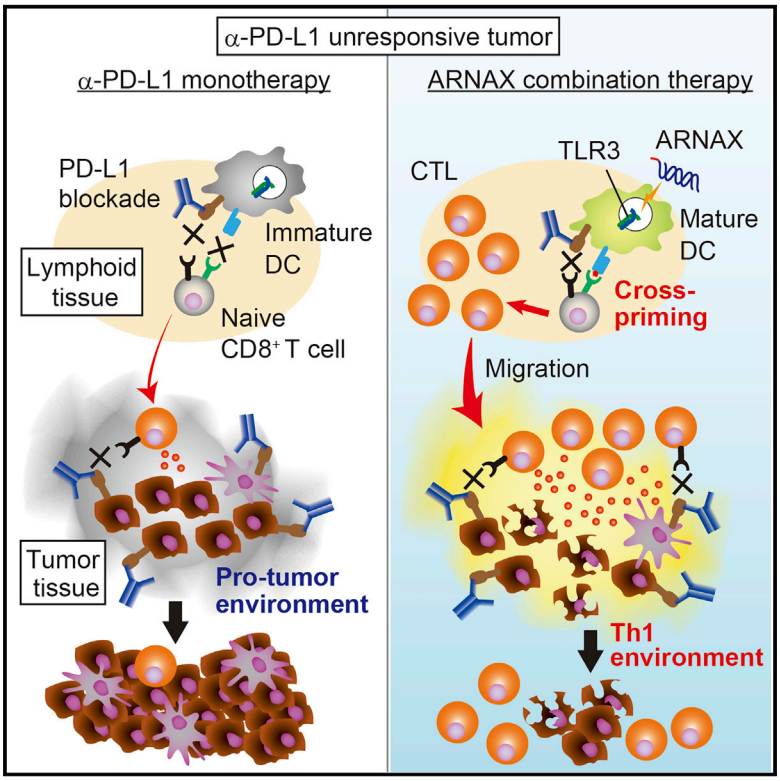

Highlights

- Vaccine immunotherapy with ARNAX and tumor antigen overcomes anti-PD-L1 resistance
- ARNAX induces anti-tumor CTLs and their infiltration into the tumor site via TLR3
- ARNAX therapy establishes Th1-type anti-tumor immunity and leads to tumor regression
- ARNAX therapy enhances anti-tumor responses in conjunction with PD-L1 blockade

Authors

Yohei Takeda, Keisuke Kataoka, Junya Yamagishi, Seishi Ogawa, Tsukasa Seya, Misako Matsumoto

Correspondence

seya-tu@pop.med.hokudai.ac.jp (T.S.), matumoto@pop.med.hokudai.ac.jp (M.M.)

In Brief

PD-1 blockade benefits a small proportion of cancer patients with pre-existing anti-tumor CTLs. Takeda et al. show that the TLR3-specific ligand, ARNAX, and tumor-associated antigens (TAAs) induce anti-tumor CTLs, establish Th1-type anti-tumor immunity, and lead to tumor regression without inflammation. Combination therapy using ARNAX/TAA and anti-PD-L1 Ab overcomes PD-1 blockade-unresponsiveness.

Takeda et al., 2017, Cell Reports *19*, 1874–1887
May 30, 2017
http://dx.doi.org/10.1016/j.celrep.2017.05.015

OPEN ACCESS
CellPress

Cell Reports
Article

A TLR3-Specific Adjuvant Relieves Innate Resistance to PD-L1 Blockade without Cytokine Toxicity in Tumor Vaccine Immunotherapy

Yohei Takeda,[1,4] Keisuke Kataoka,[2,4] Junya Yamagishi,[3,4] Seishi Ogawa,[2] Tsukasa Seya,[1,*] and Misako Matsumoto[1,5,*]
[1]Department of Vaccine Immunology, Hokkaido University Graduate School of Medicine, Kita 15, Nishi 7, Kita-ku, Sapporo 060-8638, Japan
[2]Department of Pathology and Tumor Biology, Graduate School of Medicine, Kyoto University, Kyoto 606-8501, Japan
[3]Research Center and Global Station for Zoonosis Control, GI-CoRE, Hokkaido University, Sapporo 001-0020, Japan
[4]These authors contributed equally
[5]Lead Contact
*Correspondence: seya-tu@pop.med.hokudai.ac.jp (T.S.), matumoto@pop.med.hokudai.ac.jp (M.M.)
http://dx.doi.org/10.1016/j.celrep.2017.05.015

SUMMARY

Cancer patients having anti-programmed cell death-1 (PD-1)/PD ligand 1 (L1)-unresponsive tumors may benefit from advanced immunotherapy. Double-stranded RNA triggers dendritic cell (DC) maturation to cross-prime antigen-specific cytotoxic T lymphocytes (CTLs) via Toll-like receptor 3 (TLR3). The TLR3-specific RNA agonist, ARNAX, can induce anti-tumor CTLs without systemic cytokine/interferon (IFN) production. Here, we have developed a safe vaccine adjuvant for cancer that effectively implements anti-PD-L1 therapy. Co-administration of ARNAX with a tumor-associated antigen facilitated tumor regression in mouse models, and in combination with anti-PD-L1 antibody, activated tumor-specific CTLs in lymphoid tissues, enhanced CTL infiltration, and overcame anti-PD-1 resistance without cytokinemia. The TLR3-TICAM-1-interferon regulatory factor (IRF)3-IFN-β axis in DCs exclusively participated in $CD8^+$ T cell cross-priming. ARNAX therapy established Th1 immunity in the tumor microenvironment, upregulating genes involved in DC/T cell/natural killer (NK) cell recruitment and functionality. Human ex vivo studies disclosed that ARNAX+antigen induced antigen-specific CTL priming and proliferation in peripheral blood mononuclear cells (PBMCs), supporting the feasibility of ARNAX for potentiating anti-PD-1/PD-L1 therapy in human vaccine immunotherapy.

INTRODUCTION

Blockade of the programmed cell death-1 (PD-1) immune checkpoint pathway induces efficient remission in patients with metastatic cancers (Kamphorst and Ahmed, 2013; Hamid et al., 2013; Herbst et al., 2014; Tumeh et al., 2014), but responses are observed in only ~20% of patients with all solid tumor types (Herbst et al., 2014; Tumeh et al., 2014). Preexistence of anti-tumor cytotoxic T lymphocytes (CTLs) and their infiltration into tumors are a prerequisite for treatment efficacy (Tumeh et al., 2014). The frequency of high nonsynonymous mutations in tumors is correlated with the efficacy of PD-1/PD-ligand-1 (PD-L1) blockade therapy and long-term survival of patients (Rizvi et al., 2015; Schumacher and Schreiber, 2015). Thus, mutated tumor-associated antigens (TAAs) may be involved in the generation of anti-tumor CTLs and responses to PD-1/PD-L1 blockade therapy. Tumor-specific CTLs have been characterized using TAA peptides and tetramers in peptide vaccine therapy preceding PD-1 checkpoint inhibition (Coulie et al., 2014). In patients responding to peptide vaccine therapy, tetramer-positive CTLs are increased in the blood and tumor sites. Insufficient induction of tumor-specific CTLs would have been a barrier to establishment of the vaccine therapy.

TAA-specific CTLs are generated in the draining lymph node (DLN) in line with maturation of antigen (Ag)-presenting dendritic cells (DCs), coupled with cross-priming, upregulation of major histocompatibility complex (MHC)/B7s, and production of type I interferon (IFN) and IL-12, which are induced by signals from pattern recognition receptors (Steinman and Banchereau, 2007). The majority of vaccines for infectious diseases are naturally effective because both Ag and pattern molecules (adjuvant) are simultaneously provided to satisfy the above criteria, thereby facilitating DC maturation (Seya and Matsumoto, 2009). Tumors are self-originating and essentially lack adjuvant. In the absence of adjuvant, no response is triggered against the tumor, even though PD-1/PD-L1 blockade has the potential to replenish CTLs and restore their function. Currently approved adjuvants, such as Alum and oil, deviate from the purpose for supporting tumor immunotherapy, because they are inflammasome or monocyte/macrophage stimulators (Eisenbarth et al., 2008; Mbow et al., 2010). The development of appropriate priming adjuvants remains an urgent medical need to optimize the high efficacy of checkpoint therapy.

Poly(I:C) is an adjuvant that targets DCs in DLN and tumor microenvironments and converts them into the active phenotype, inducing priming and proliferation of tumor-specific CTLs and

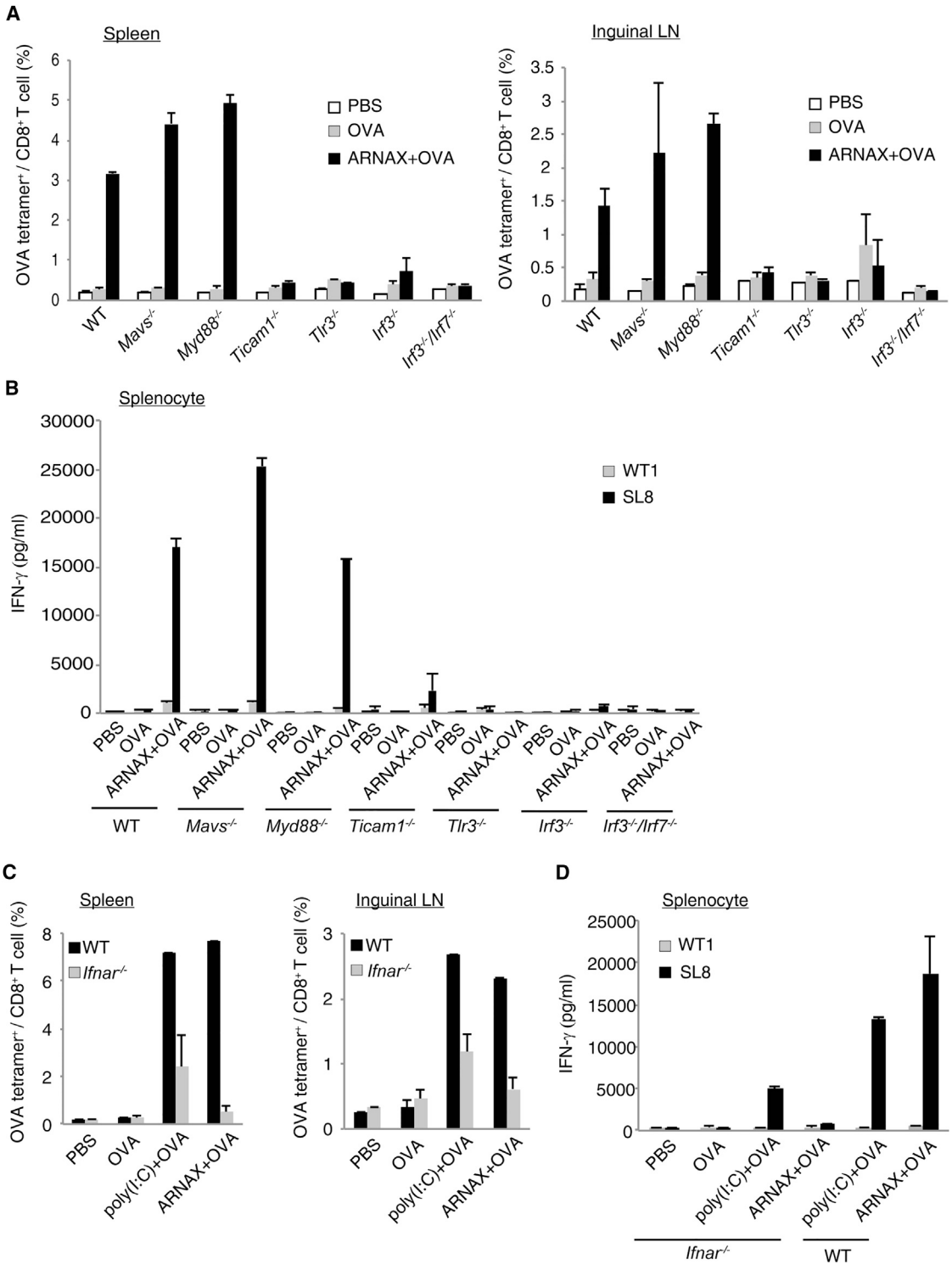

Figure 1. The TLR3-TICAM-1-IRF3-IFN-β Axis in DCs Is Indispensable for ARNAX-Induced Ag-Specific CD8⁺ T Cell Priming

(A) OVA-specific CD8⁺ T cell proliferation in spleen and inguinal LN from wild-type and knockout mice. Mice were injected s.c. with PBS, OVA, or ARNAX+OVA on days 0 and 7 (n = 2 per treatment). On day 11, OVA-specific CD8⁺ T cell proliferation in spleen (left) and inguinal LN (right) was evaluated with the tetramer assay. Error bars indicate means ± SD. Data are representative of two independent experiments.

(B) IFN-γ production by OVA-specific CD8⁺ T cells in spleen cells. Spleen cells were stimulated with OVA (SL8) or WT1 (Db126) peptide for 3 days and the IFN-γ level in the culture supernatant was measured using CBA.

(legend continued on next page)

altering the microenvironment from tumor-supporting to tumor-suppressive (Azuma et al., 2012, 2016; Shime et al., 2012, 2017). Numerous clinical trials have been conducted with poly(I:C) (Galluzzi et al., 2012). One critical point of poly(I:C) is to provoke systemic cytokine toxicity (Levine et al., 1979; Lampkin et al., 1985). Minimal doses have been applied to prime DCs with the aim of reducing toxicity, but safe amounts appear insufficient to evoke the immune response, determined by CTL quality (Sabbatini et al., 2012). To guarantee proliferation and high quality of anti-tumor CTLs as well as efficacy of checkpoint therapy in non-responsive cancer patients, we should establish non-toxic priming-phase adjuvants and then construct a synergistic therapy with anti-PD-1/PD-L1 Ab.

Comprehensive genomic and transcriptomic studies have been conducted on several tumors to determine the features affecting sensitivity or resistance to checkpoint blockade therapy (Zelenay et al., 2015; Hugo et al., 2016). Innate resistance properties of non-responding tumors (Hugo et al., 2016) as well as immunosuppressive tumor microenvironments (Zelenay et al., 2015) appear to affect the efficacy of checkpoint blockade, and combination strategies targeting these negative factors have been proposed to overcome anti-PD-1 resistance (Gajewski et al., 2013; Sharma and Allison, 2015a; Salmon et al., 2016; De Henau et al., 2016). However, effective measures to overcome the unresponsiveness to PD-1 blockade in patients with lower nonsynonymous mutation burden in tumors or low levels of anti-tumor CTLs remain to be established.

Here, we explored the utility of combination therapy with anti-PD-L1 Ab and the non-inflammatory adjuvant, ARNAX, targeting endosomal Toll-like receptor 3 in DCs in a mouse tumor model (Matsumoto et al., 2015; Seya et al., 2015). Toll-like receptor 3 (TLR3) is highly expressed in professional Ag-presenting mouse CD8α^+ and CD103$^+$ and human CD141$^+$ DCs (Bachem et al., 2010; Jongbloed et al., 2010). ARNAX co-administered with TAA facilitated tumor regression in mouse tumor implant models, and in combination with anti-PD-L1 Ab, promoted full priming of anti-tumor CTLs and proliferation in DLN and enhanced CD8$^+$ T cell infiltration into the tumor site, leading to relief against anti-PD-1 unresponsiveness. Throughout the therapy, ARNAX elicited efficient anti-tumor immunity with no cytokinemia.

RESULTS

The TLR3-TICAM-1-Interferon Regulatory Factor 3-IFN-β Axis in DCs Is Essential for Ag-Specific CTL Priming by ARNAX

The TLR3-specific adjuvant consisting of 140 bp double-stranded RNA (dsRNA) capped with phosphorothioated oligodeoxynucleotides, designated ARNAX, can induce anti-tumor CTLs without systemic cytokine/IFN production (Matsumoto et al., 2015). Here, we determined the signaling cascade of ARNAX-induced cross-priming using mice depleted of innate immune receptors/signaling molecules (Figure 1). ARNAX failed to induce ovalbumin (OVA)-specific CD8$^+$ T cell proliferation and IFN-γ production in spleen and inguinal LN of *Tlr3*$^{-/-}$, *Ticam1*$^{-/-}$, *Irf3*$^{-/-}$, and *Irf3*$^{-/-}$/*Irf7*$^{-/-}$ mice (Figures 1A, 1B, and S1A). In contrast, knockout of *Mavs* (an adaptor for RIG-I/MDA5) or *Myd88* (an adaptor for TLRs, except TLR3) did not affect ARNAX-induced CD8$^+$ T cell priming (Figures 1A, 1B, and S1A), indicating that the TLR3-TICAM-1-interferon regulatory factor 3 (IRF3) axis is indispensable for ARNAX-induced cross-priming. ARNAX appears to escape from recognition by the RNA sensors, RIG-I and MDA5, and the DNA sensor, TLR9.

Accumulating evidence suggests that type I IFN-signaling is critical for cross-priming in DCs (Fuertes et al., 2011, 2013; Pantel et al., 2014). In *Ifnar*$^{-/-}$ mice, ARNAX hardly induced OVA-specific CD8$^+$ T cell proliferation in spleen and inguinal LN, whereas poly(I:C) that activates both TLR3 and MDA5 (Kato et al., 2006; Matsumoto and Seya, 2008) induced proliferation even in the absence of type I IFN signaling (Figures 1C and S1B). In accordance with this finding, splenocytes from ARNAX+OVA-treated *Ifnar*$^{-/-}$ mice secreted little or no IFN-γ upon re-stimulation with OVA-specific SL8 peptide in vitro (Figure 1D). The finding that ARNAX induces IFN-β mRNA expression in lymphoid tissues without systemic type I IFN production (Matsumoto et al., 2015) suggests that the TLR3-TICAM-1-IRF3-IFN-β axis in DCs exclusively participates in ARNAX-mediated CD8$^+$ T cell priming.

Features of ARNAX-Induced Cytokine Production

Cytokines, including IL-12 and type I IFN, are required for CD8$^+$ T cell priming as a third signal for the development of functional T cells (Curtsinger and Mescher, 2010; Gerner et al., 2013). Accordingly, we examined the cytokine profile induced upon subcutaneous (s.c.) injection of ARNAX in mice. IL-6, tumor necrosis factor alpha (TNF-α), and IFN-β levels induced by ARNAX were lower than those induced by poly(I:C) (Figure 2A). Recently, we showed that intraperitoneal (i.p.) injection of poly(I:C) in mice induced robust serum IL-6, TNF-α, and IFN-β production, whereas minimal or no induction was observed following i.p. administration of ARNAX (Matsumoto et al., 2015). The results were reproducible with those obtained upon intravenous (i.v.) injection, ARNAX barely induced IL-6, TNF-α, and IFN-β production in contrast to poly(I:C) (Figure 2B), reflecting its non-inflammatory properties. Notably, the Th1 cytokine, IL-12p40, and chemokine, IP-10, that recruits natural killer (NK) cells and CTLs were substantially induced upon s.c. injection of ARNAX, similar to data obtained with poly(I:C) (Figure 2A), implying that ARNAX mediates Th1 skewing with less inflammation. Given that IL-12-stimulated CD8$^+$ T cells express lower levels of PD-1 upon re-encountering Ag in tumors and survive longer than type I IFN-stimulated T cells (Gerner et al., 2013), the ARNAX-induced cytokine profile of IL-12^{high}/IFN-β^{low} may be an advantage for CD8$^+$ T cells in controlling tumors.

(C) ARNAX-induced cross-priming is dependent on the type I IFN signal. Wild-type and *Ifnar*$^{-/-}$ mice were injected s.c. with PBS, OVA, poly(I:C)+OVA, or ARNAX+OVA (n = 2 per treatment). Data are representative of two independent experiments.
(D) IFN-γ production by OVA-specific CD8$^+$ T cells in spleen. Error bars indicate mean values ± SD.
See also Figure S1.

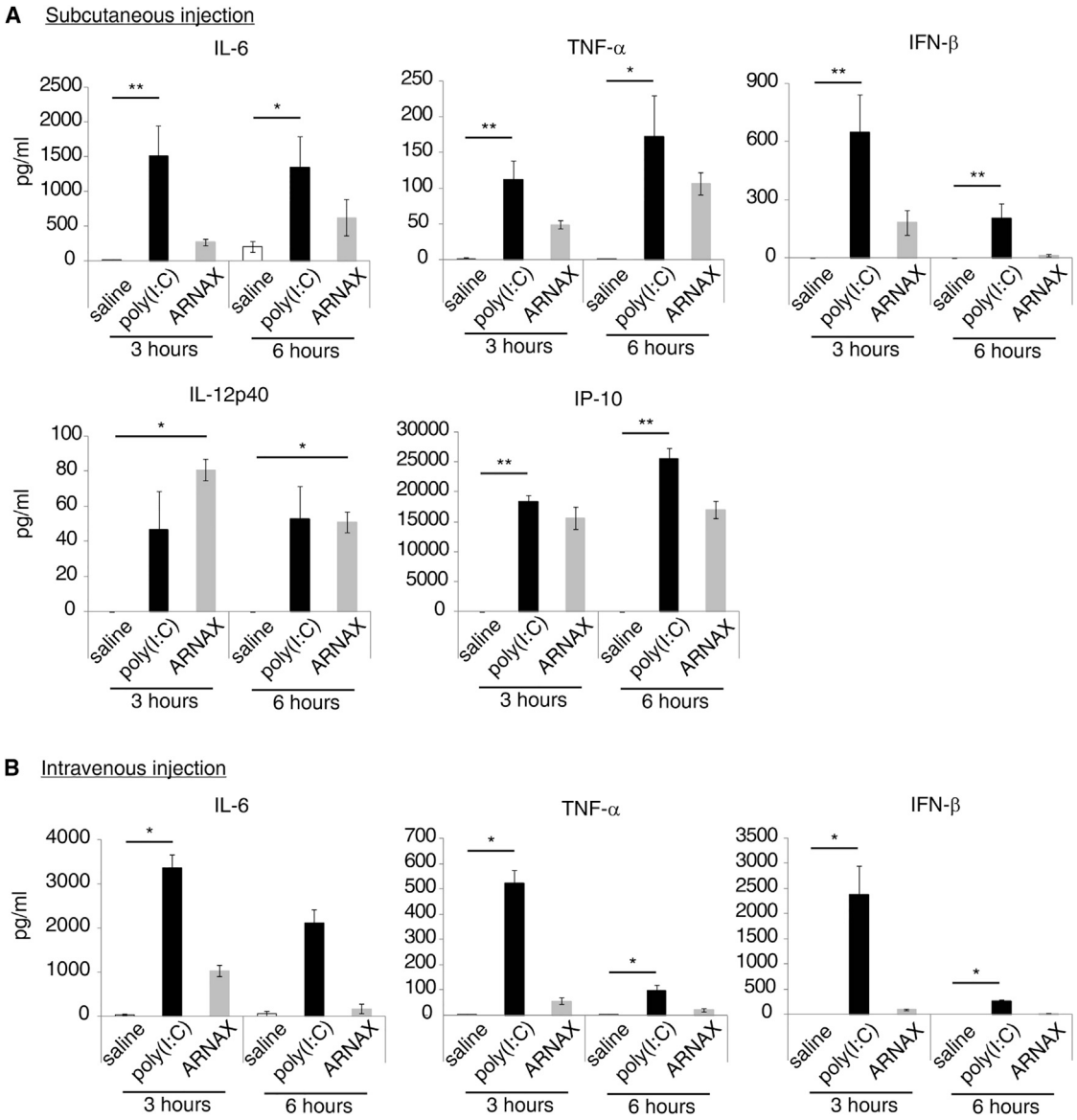

Figure 2. ARNAX Induces Th1 Cytokines with Lower IFN-β Production

Wild-type mice were injected s.c. with saline (n = 4), 150 μg poly(I:C) (n = 5), or ARNAX (n = 4) (A) or i.v. with saline, 50 μg poly(I:C), or ARNAX (B) (n = 3 per treatment). At timed intervals, blood was collected from the tail vein and cytokine levels in each sample were measured with CBA or ELISA. Data are presented as means ± SEM. *p < 0.05, **p < 0.01, Kruskal-Wallis test with Dunn's multiple comparison test.

ARNAX with TAA Induces Anti-tumor Immunity in PD-1/PD-L1 Blockade-Unresponsive Tumors

Multiple human cancers display aberrant PD-L1 expression on the cell surface (Kataoka et al., 2016), and PD-1 therapy has mainly been applied for cancer patients with PD-L1-expressing tumors. However, not all tumors expressing PD-L1 respond to PD-1 blockade, and the response to PD-L1 therapy cannot be predicted from *PD-L1* levels in tumors (Hugo et al., 2016). To determine the ability of ARNAX to induce anti-tumor CTLs that can overcome anti-PD-1 resistance irrespective of the PD-L1 level, vaccine immunotherapy using ARNAX and tumor Ag (OVA) was conducted against mouse EG7 (OVA-expressing EL4 lymphoma) tumors with low or high PD-L1 levels (Kataoka et al., 2016). We first examined in vivo targets of ARNAX in PD-L1^{lo} EG7-bearing mice. ARNAX stimulated splenic CD8α^{+} and CD8α^{-} DCs to produce IL-12p40 and TNF-α (Figure S2A). In addition, CD11c^{lo}CD11b^{+} myeloid cells produced TNF-α in response to ARNAX (Figure S2A).

PD-L1^{lo} EG7 tumors are unresponsive to anti-PD-L1 Ab and efficiently reduced with s.c. injection of ARNAX+OVA (Figures 3A–3C and S3A–S3C). CD8^{+} T cells infiltrated the tumor site, and OVA tetramer-positive CD8^{+} T cells were enriched compared to PBS injection (Figures 3D and 3E). CD11c^{+}CD8^{+} T cells, an active phenotype of effector CTLs, (Takeda et al.,

2016) were increased upon ARNAX+OVA treatment (Figure 3D). ARNAX+OVA therapy significantly upregulated mRNA expression of the genes related to CTL activation and cytotoxicity (*Ifng*, *Gzmb*, and *Prf1*) and chemokines recruiting the CTLs (*Cxcl9* and *Cxcl10*) in tumors (Figure 3F). Furthermore, *Tbx21* and *Il12b* mRNA levels were upregulated, indicating Th1-type anti-tumor immunity (Zelenay et al., 2015).

ARNAX with TAA in Combination with Anti-PD-L1 Ab Induces Anti-tumor Immunity against PD-L1-High Tumors

Next, we devised a combination therapy with ARNAX+OVA and anti-PD-L1 Ab against EG7 tumors expressing high levels of PD-L1 (Figures 4A and 4B). Anti-PD-L1 Ab treatment failed to induce PD-L1^{hi} tumor retardation (Figure 4C). In contrast, ARNAX+OVA therapy suppressed tumor growth despite high PD-L1 expression, and co-administration of anti-PD-L1 Ab enhanced the ARNAX-mediated anti-tumor response (Figure 4C). Following ARNAX+OVA therapy, OVA-specific CD8$^+$ T cells were modestly induced in spleen and significantly increased in tumors, resulting in tumor regression (Figure 4D). PD-L1 blockade did not induce OVA-specific CD8$^+$ T cells in spleen, while combination with ARNAX+OVA more strongly facilitated OVA-specific CD8$^+$ T cell priming in spleen and infiltration of CD8$^+$ T cells into the tumor site than ARNAX+OVA treatment alone. The activation marker, CD11c, and the PD-1-positive CD8$^+$ T cells were also increased in spleen following combination therapy. Furthermore, intratumoral mRNA expression of *Gzmb*, *Ifng*, *Prf1*, and *Cxcl9* was upregulated by ARNAX+OVA and combination therapy (Figure 4E). These results collectively suggest that ARNAX serves as a priming adjuvant to induce Ag-specific CD8$^+$ T cells in lymphoid tissues, and blockage of the PD-1/PD-L1 pathway augments ARNAX-mediated CD8$^+$ T cell activation and infiltration into the tumor site, where CTL function is restored.

The augmentation of Ag-specific CD8$^+$ T cell priming in spleen following ARNAX+OVA/anti-PD-L1 Ab treatment was also observed in PD-L1^{lo} EG7 tumors, although ARNAX+OVA single therapy was sufficient for tumor regression (Figure S3). PD-L1 is expressed on APCs and upregulated by inflammatory signals (Keir et al., 2008; Schietinger and Greenberg, 2014; Joyce and Fearon, 2015; Zou et al., 2016). We examined the in vivo expression of PD-L1 on APCs in lymphoid tissues and tumors in PD-L1^{lo} EG7-bearing mice. In spleen and DLN, DC subsets including CD8α^+, CD8α^- DCs and pDCs, CD11b$^+$Ly6C$^+$ cells, and macrophages expressed low or median levels of PD-L1, while CD11b$^+$Ly6G$^+$ cells did not (Figure S2B). In contrast, tumor-associated DCs and CD11b$^+$ myeloid cells all expressed high levels of PD-L1, in particular, CD8α^+ DCs, CD11b$^+$Ly6G$^+$, and CD11b$^+$Ly6C$^+$ cells dramatically increased PD-L1 expression (Figure S2B). Thus, PD-1 pathway blockade may enhance TAA-specific CD8$^+$ T cell proliferation induced by ARNAX+TAA at the priming phase. The different effect of ARNAX+OVA single therapy on PD-L1-low or -high EG7 tumors appears to reflect PD-L1 levels on tumors, not on tumor-infiltrated cells (Figures 3 and 4). Synergistic effect of combination therapy was also obtained with another mouse tumor model, MO5 (OVA-expressing B16 melanoma cell line) (Figure S4). While anti-PD-L1 Ab or ARNAX+OVA single therapy only partially suppressed tumor growth, combination treatment induced additive regression of MO5 tumors (Figures S4A–S4C). Increased level of tumor-specific CTLs in spleen and upregulation of intratumoral mRNA expression of *Gzmb*, *Ifng*, *Prf1*, *Cxcl9*, and *Cxcl10* were reproducibly observed following combination therapy with ARNAX+OVA and anti-PD-L1 Ab (Figures S4D and S4E).

Notably, in mouse tumor model WT1-C1498 (an acute lymphoma cell line overexpressing WT1), ARNAX significantly suppressed tumor growth without co-administration of TAA (Figures S5A–S5D). CD8$^+$ T cells infiltrated into the tumors and CD8$^+$ T effector population (CD62L$^-$CD11c$^+$PD-1$^+$) were increased (Figure S5E). PD-L1 blockade elicits tumor rejection regardless of combination with ARNAX. In these settings, CD8$^+$ T cells infiltrated the tumor site, and CD8$^+$ T effector population was increased in both spleen and tumors (Figure S5E). An intriguing notion is that spontaneous tumor-specific CD8$^+$ T cell priming occurs in lymphoid tissues, which is enhanced by PD-L1 blockade, resulting in CD8$^+$ T cell infiltration into tumors. ARNAX appears to boost Ag-specific CTL priming together with intrinsic tumor Ag released from damaged tumor cells (Kroemer et al., 2013).

ARNAX Therapy Changes the Tumor-Infiltrating Immune Cell Population from Immune Suppressive to Effective

Tumor growth is promoted by inflammation in the tumor microenvironments infiltrated by immune cells (Coussens et al., 2013; Mantovani et al., 2008). We assessed the tumor-infiltrating immune cell population in ARNAX-treated EG7 tumors (CD45.2$^+$) following poly(I:C)+OVA or ARNAX+OVA treatment using CD45.1 congenic mice as the host (Figures 5A, S6A, and S6B). Administration of ARNAX or poly(I:C) together with OVA led to a significant increase in the CD8$^+$ T cell proportion of CD45.1$^+$ cells within the tumor region (PBS, ~5%, ARNAX or poly(I:C)+OVA, >20%) as well as a mild increase in the NK cell population (Figure 5B). CD4$^+$ T, NKT, and B cells represented a minor population in tumor regions (Figures 5B and S6C). Among DC subsets that were also minor populations, the CD8α^+ DC population was largely increased following ARNAX or poly(I:C)+OVA therapy, while the proportion of pDC, CD103$^+$ DC, and CD4$^+$ DC remained unchanged (Figures 5C, S6D, and S6E). Conversely, the CD11b$^+$ myeloid cell population accounting for >60% CD45.1$^+$ cells in the untreated tumor region was decreased by ARNAX treatment (Figure 5D). Notably, among the CD11b$^+$ myeloid cells (including Ly6G$^+$, Ly6C$^+$, and F4/80$^+$ cells), CD11b$^+$Ly6G$^+$ cells, referred to as granulocytic myeloid-derived suppressor cells (G-MDSC) or tumor-associated neutrophils, were markedly reduced by ARNAX or poly(I:C)+OVA therapy (Figure 5D) (Peranzoni et al., 2010; Youn et al., 2008). The proportion of tumor-infiltrating myeloid cells depends on the tumor cell type. MO5 tumors are CD11b$^+$Ly6G$^+$-low and CD11b$^+$Ly6C$^+$-high, which remained unchanged, but CD8$^+$ T cells and CD8α^+ DCs were increased in the tumors following ARNAX therapy (Figure S4F). Thus, ARNAX appears to facilitate infiltration of Th1-type immune cells into the tumor site, accompanied by reduction of immunosuppressive myeloid cell recruitment.

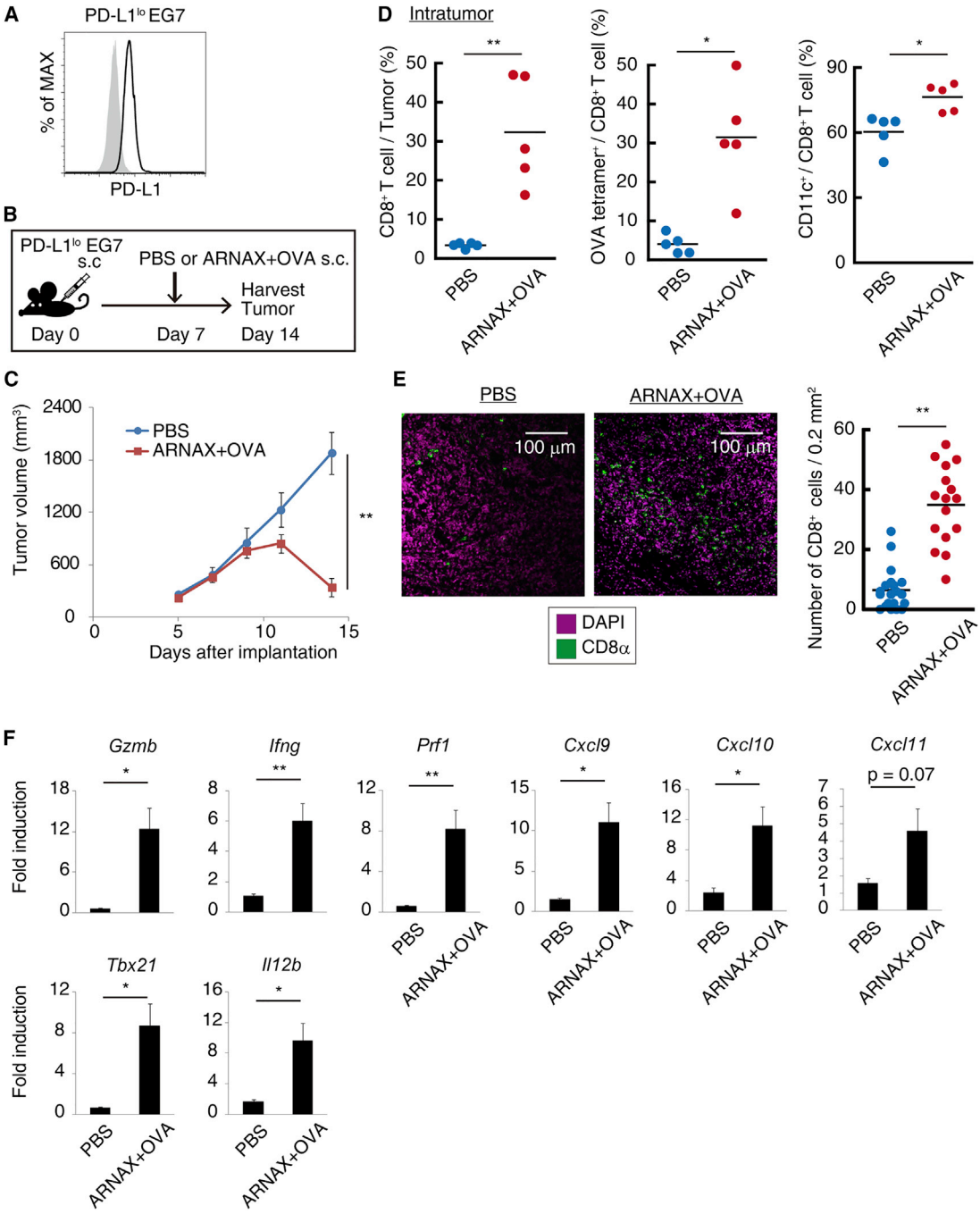

Figure 3. ARNAX and TAA Therapy Induces Tumor Regression in PD-1 Blockade-Unresponsive EG7 Tumors

(A) PD-L1 expression on PD-L1^{lo} EG7 cells. Shaded and open histograms represent isotype control and PD-L1 staining, respectively.

(B) Scheme of ARNAX+OVA therapy in PD-L1^{lo} EG7 tumors.

(C) Mice were challenged with PD-L1^{lo} EG7 cells, and 7 days later they were injected s.c. with control PBS (blue) or ARNAX+OVA (red). Tumor size was evaluated in each group. Error bars indicate means ± SEM; n = 5 per group. **p < 0.01 with Student's t test.

(D–F) On day 14, tumors were harvested from PBS- or ARNAX+OVA-treated mice and analyzed. (D) Flow cytometry analysis of tumor-infiltrating CD8$^+$ T cells (left), OVA-specific CD8$^+$ T cell proliferation (center), and CD11c expression on CD8$^+$ T cells (right). n = 5 per group. (E) Left: representative confocal images of tumor-infiltrating CD8$^+$ cells (green) in PBS- or ARNAX+OVA-treated mice. Scale bar, 100 μm. Right: the number of tumor-infiltrating CD8$^+$ cells per 0.2 mm^2 field was counted in random confocal images from two to three animals per group (PBS, 20 images; ARNAX+OVA, 16 images). (F) Gene expression analysis in tumors from PBS- or ARNAX+OVA-treated mice. Indicated mRNA levels were measured using qPCR and normalized to *Gapdh*. Error bars indicate means ± SEM; n = 5 per group. *p < 0.05, **p < 0.01 with Student's t test.

See also Figures S2 and S3.

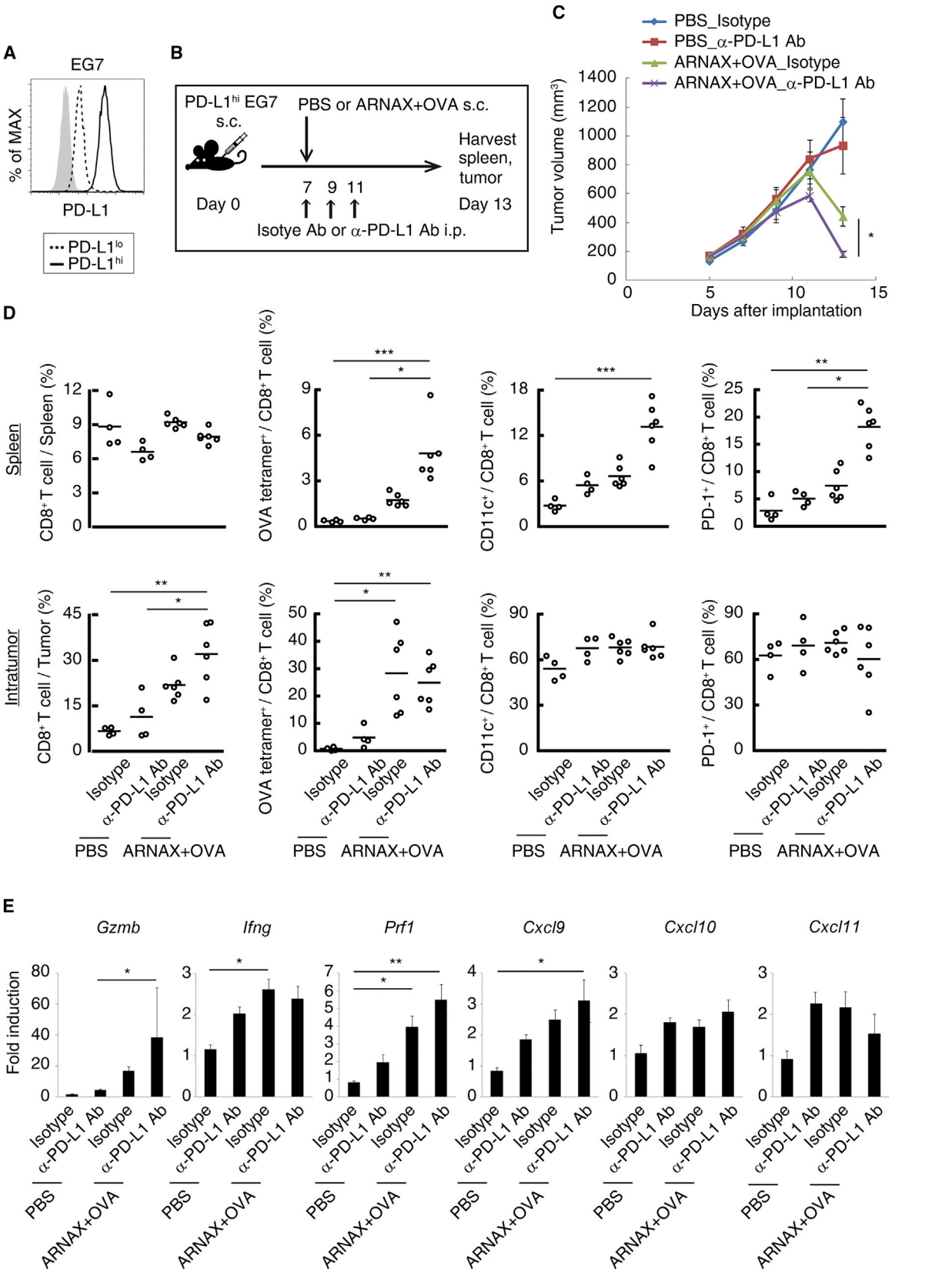

(legend on next page)

ARNAX Induces Th1-type Anti-tumor Immunity in the Tumor Microenvironment

To examine ARNAX-mediated anti-tumor immunity, comprehensive gene expression analysis was performed via RNA sequencing of whole EG7 tumors treated with PBS, ARNAX+OVA, or poly(I:C)+OVA. To evaluate early and late tumor responses, we harvested whole tumor tissues on 18 hr and 6 days after adjuvant+OVA injection (Figures 6A and S7A). On day 8 (18 hr after the treatment), we observed no differences in tumor growth among the groups with PBS, ARNAX+OVA, and poly(I:C)+OVA (Figure S7B). Overall, no significant variations in gene expression were observed among the three groups under the 18 hr conditions (Figure S7C). Some of IFN-inducible genes, however, were significantly upregulated in the poly(I:C)+OVA group (Figures S7D and S7E) but not the ARNAX+OVA group, which showed no significant variation in these gene expressions compared to the PBS group (data not shown), suggesting that ARNAX barely induces type I IFN even in the tumor microenvironment. On day 13, tumor growth was similarly retarded in response to ARNAX+OVA and poly(I:C)+OVA therapy (Figure 6B). Concomitantly, numerous genes related to anti-tumor immunity were upregulated in the ARNAX+OVA and poly(I:C)+OVA groups (Figures 6C and 6D). In particular, chemokine genes, including *Ccl4*, *Ccl5*, *Ccl8*, and *Ccl27*, were significantly increased in response to TLR3 agonists (Figure 6D). Their receptor genes are expressed in DCs, NK, and T cells (Bachmann et al., 2006), which may account for accumulation of CD8α^+ DCs, T cells, and NK cells in the tumors (Figures 5B and 5C). In addition, NK/T cell function-related genes and cell adhesion genes, such as *Vcam1*, were upregulated (Figure 6D). On the other hand, NK cell inhibitory receptor *Klra1* (Ly49 receptor), and *Tnfsf4* (OX40L) involved in Th2 cell differentiation, were downregulated with ARNAX/poly(IC)+OVA therapy. Ag-presenting cell-related genes were augmented to accelerate T cell priming. Significant correlation between the expression levels of these genes on day 13 and tumor growth retardation was observed (Figures 6B and 6D). No significant variations in gene expression were observed between ARNAX+OVA and poly(I:C)+OVA treatment groups on day 13 (Figure 6E). Taken together, these results strongly suggest that ARNAX therapy modulates the tumor microenvironment and elicits Th1-type anti-tumor immunity with minimal essential cytokine induction.

ARNAX Induces Ag-Specific CTLs in Human Peripheral Blood Mononuclear Cells

To determine whether ARNAX induces Ag-specific CD8$^+$ T cell priming in humans as observed for mice, we employed a cytomegalovirus (CMV)-tetramer assay using human peripheral blood mononuclear cells (PBMCs). PBMCs isolated from individual healthy donors were stimulated with ARNAX or poly(I:C) with or without the CMV pp65 protein. In the absence of Ag (CMV pp65), poly(I:C) and ARNAX did not significantly promote CMV pp65-specific CD8$^+$ T cell expansion (Figure 7). In the presence of CMV pp65 Ag, pp65-specific CD8$^+$ T cells were expanded even without adjuvant, to different extents among individuals. Remarkably, the proportion of pp65 tetramer-positive cells was considerably increased upon simultaneous stimulation with adjuvant and pp65 Ag, compared to Ag only. The degree of pp65-specific CD8$^+$ T cell expansion induced by ARNAX+Ag was comparable to that induced by poly(I:C)+Ag. These results support the ability of ARNAX to induce Ag-specific CD8$^+$ T cells in in vitro human PBMC systems.

DISCUSSION

Immunotherapy with PD-1/PD-L1 blockade has provided a breakthrough in cancer treatment. However, additional therapeutic strategies are necessary to improve the remission rates in non-responding patients with solid tumors. Here, we aimed to develop a safe vaccine immunotherapy for cancer that effectively implements anti-PD-L1 immunotherapy. ARNAX and TAA bimodally contribute to tumor regression by inducing tumor-specific CTLs in lymphoid tissues and facilitating their infiltration into the tumor site. ARNAX satisfies cross-priming of CTL by DCs in lymphoid tissues with minimal essential cytokine induction in contrast to poly(I:C). Type I IFN-signaling in DCs is indispensable for CD8$^+$ T cell priming (Fuertes et al., 2011, 2013; Pantel et al., 2014): even locally secreted type I IFN is sufficient for ARNAX-mediated cross-priming. In addition, ARNAX induces Th1-type chemokines, CXCL9 and CXCL10, that recruit CXCR3$^+$CD8$^+$ T cells to the tumor site. CXCR3 levels on T cells are high in DLNs while low in tumors, which allows the T cells to stay in tumors (Sistigu et al., 2014). These innate features of ARNAX can overcome anti-PD-1 resistance that is associated with insufficient anti-tumor CD8$^+$ T cell priming and limited tumor CD8$^+$ T cell infiltration (Tumeh et al., 2014; Sharma and Allison, 2015b). ARNAX administered with TAA facilitates PD-L1 Ab activity in tumor regression in mouse implant tumor models. In the effector phase, tumor cells and tumor-associated APCs express PD-L1 to prevent CTL attack. In the priming phase, PD-L1 is expressed on Ag-presenting DCs and macrophages. Curiel et al. (2003) reported that tumor environmental factors upregulates PD-L1 expression on DCs in tumors and tumor draining

Figure 4. ARNAX+OVA Synergistically Induce Anti-tumor Immunity with PD-L1 Ab in PD-L1^{hi} EG7 Tumors

(A) Comparison of surface PD-L1 expression between PD-L1^{lo} and PD-L1^{hi} EG7 cells. Dotted and solid lines signify PD-L1 expression in PD-L1^{lo} EG7 and PD-L1^{hi} EG7 cells, respectively. The shaded histogram represents isotype control Ab staining.

(B) Scheme of combination therapy of ARNAX+OVA and anti-PD-L1 Ab in PD-L1^{hi} EG7 tumors.

(C) PD-L1^{hi} EG7-bearing mice were treated with PBS (n = 4) or ARNAX+OVA (n = 6) in combination with anti-PD-L1 Ab or isotype control Ab as shown in (B), and tumor sizes were evaluated in each group. Error bars indicate means ± SEM. *p < 0.05 with Student's t test.

(D) CD8$^+$ T cell density, OVA-specific CD8$^+$ T cell proliferation, and the proportion of CD8$^+$ T cells expressing CD11c or PD-1 in spleen (top) and intratumors (bottom).

(E) Gene expression analysis in tumors harvested from tumor-bearing mice on day 13 in each group. Indicated mRNA levels were measured with qPCR and normalized to *Gapdh*. Error bars indicate means ± SEM; n = 4 or 6 per group. *p < 0.05, **p < 0.01, ***p < 0.001 with Kruskal-Wallis test with Dunn's multiple comparison test (D and E).

See also Figures S2–S5.

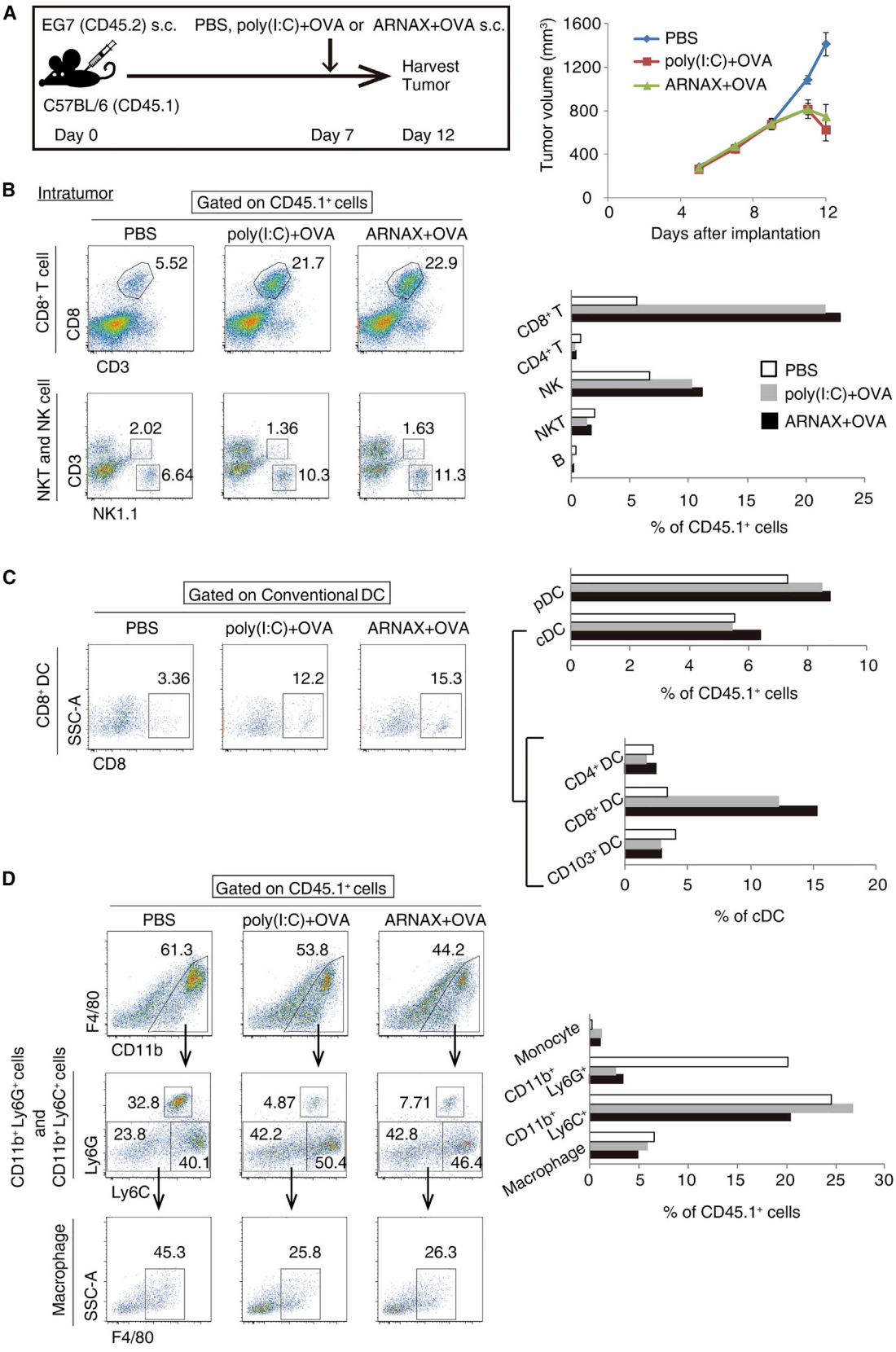

(legend on next page)

LN, which impairs DC-mediated T cell activation. Hence, blocking of PD-L1 promotes ARNAX-driven proliferation of Ag-specific $CD8^+$ T cells and tumor cytotoxicity in the priming and effector phases, respectively.

Anti-tumor $CD8^+$ T cells induced by ARNAX exhibit an effector T cell phenotype (Kaech and Cui, 2012), whereby cell surface CD11c and PD-1 are increased concomitantly with cytotoxicity-related genes, *Gzmb, Prf1*, and *Ifng.* In addition, the transcription factor, *Tbx21*, is upregulated to skew effector T cells. Data from RNA sequencing (RNA-seq) revealed that Th1-type anti-tumor immunity is established in EG7 tumor microenvironment following ARNAX/TAA therapy. In particular, chemokines related to the recruitment of $CD8\alpha^+$ DCs, T and NK cells, many NK/T cell function-related molecules, and Ag-presenting cell-related molecules are significantly increased in tumors following ARNAX+OVA treatment. Interestingly, the expression levels of these genes and tumor growth retardation were significantly correlated. Thus, efficient induction of Th1-type anti-tumor immunity requires DC-priming adjuvant supporting TAA. ARNAX and poly(I:C) brought similar gene expression profiles in the tumor microenvironment. However, poly(I:C) induces systemic cytokinemia in i.v. and i.p. injection, while ARNAX does not in any route of injection. Furthermore, expression of type I IFN and IFN-inducible genes that trigger inflammation in tumors was barely induced following ARNAX+OVA treatment.

Innate-resistance features of non-responding tumors and immunosuppressive tumor microenvironments are reported to negatively affect anti-PD-1 therapy (Zelenay et al., 2015; Hugo et al., 2016; De Henau et al., 2016). ARNAX therapy participates in modulation of the tumor microenvironment to drive effective anti-tumor immunity. Ultimately, ARNAX licenses DCs in tumors and DLN to activate functional tumor-specific CTLs and relieve anti-PD-L1 unresponsiveness. In MO5 and WT1-C1498 tumor models, anti-PD-L1 Ab was partially or highly effective in tumor regression, suggesting the preexistence of tumor-reactive CTLs. Indeed, intratumor $CD8^+$ T cell population in PBS-treated MO5 or WT1-C1498 tumors was higher than that in PBS-treated EG7 tumors where tumor-reactive CTLs might be less present ($\sim$10% versus $\sim$5%).

Somatic mutation and their associated antigen in the tumor genome cannot be determined without genetic analysis. TAAs are mounted on MHC under restriction of haplotypes. Priming adjuvants trigger TAA-specific CTLs in the context of MHC restriction. Investigations of TAA-selecting programs are reportedly in progress. Application of ARNAX to well-established peptide vaccine immunotherapy and/or combination with PD-1 blockade appears to present a promising strategy to overcome PD-1 resistance. In contrast to poly(I:C) that has been used for earlier clinical trials (Levine et al., 1979; Lampkin et al., 1985), ARNAX is non-toxic features and may prevent the onset of severe adverse effects that occur due to systemic inflammatory cytokine/type I IFN production. Ex vivo studies using human PBMCs showed that ARNAX and Ag induced Ag-specific CTL priming and proliferation. Because the CMV-pp65 assay has limitations in translational value, in future experiments we will design the in vitro assay to detect TAA-specific CTLs. In summary, we have presented an approach using the priming adjuvant that promotes TAA-specific expansion of CTLs and effective tumor regression in combination with checkpoint inhibitors.

EXPERIMENTAL PROCEDURES

Mice

C57BL/6 mice were purchased from CLEA Japan, and C57BL/6(CD45.1) mice were from Sankyolabo Co. *Ticam-1*$^{-/-}$ and *Mavs*$^{-/-}$ mice were generated in our laboratory and backcrossed more than eight times to adapt the C57BL/6 background. *Tlr3*$^{-/-}$ and *Myd88*$^{-/-}$ mice were kindly provided by Dr. S. Akira (Osaka University) and *Irf3*$^{-/-}$, *Irf7*$^{-/-}$ and *Ifnar*$^{-/-}$ mice by Dr. T. Taniguchi (University of Tokyo). *Irf3/Irf7* double knockout mice were generated in our laboratory by crossing *Irf3*$^{-/-}$ with *Irf7*$^{-/-}$ mice. Mice were maintained under specific pathogen-free conditions in the animal facility of Hokkaido University Graduate School of Medicine. All animal experiments were approved by the Institutional Animal Care and Use Committee of Hokkaido University and performed in compliance with their guidelines.

Cells, Reagents, and Antibodies

EG7 cells were purchased from ATCC and cultured in RPMI1640 supplemented with 10% FCS, 55 μM 2-ME, 10 mM HEPES, 1 mM sodium pyruvate, 50 IU penicillin/50 μg/mL streptomycin, and 0.5 mg/mL G418. PD-$L1^{lo}$EG7 and PD-$L1^{hi}$EG7 (mock- and sgPd-l1-transfected EG7) cells were prepared as described earlier (Kataoka et al., 2016). MO5 (Ryu et al., 2014) and WT1-C1498 were kindly provided by Dr. H. Udono (Okayama University) and H. Sugiyama (Osaka University), respectively. Poly(I:C) was purchased from Amersham Biosciences. Endotoxin-free OVA (EndoOVA) was obtained from Hyglos. $OVA_{257–264}$ peptide (SL8), WT1 peptide (Db126), OVA ($H2K^b$-SL8) tetramer, HCMV pp65 peptides, and HLA-A*02:01 and HLA-A*24:02 CMV pp65 tetramers were purchased from MBL. HCMV pp65-recombinant protein and human FcR blocking reagent were from Miltenyi Biotec. ARNAX was generated as described (Matsumoto et al., 2015), with slight modifications, whereby anti-sense 140-mer RNA was successively generated with an RNA synthesizer (GeneDesign). The antibodies used for flow cytometry analysis are listed in Table S1.

In Vivo Cross-Priming Assay

Wild-type (WT) or knockout mice (9–12 weeks) were injected subcutaneously (s.c.) with 50 μL of 100 μg EndoOVA in PBS (–) with or without 50 μL of 60 μg ARNAX twice per week. PBS (–) (100 μL) was used as the control. Spleen and inguinal LN cells were harvested 4 days after the last adjuvant injection and OVA-specific $CD8^+$ T cell proliferation was analyzed with the tetramer assay. To evaluate cytokine production, splenocytes (2×10^6/200 μL/well) were cultured for 3 days in the presence of 100 nM OVA peptide (SL8: SIINFEKL)

Figure 5. TLR3 Adjuvant Promotes Accumulation of $CD8^+$ T Cells and $CD8\alpha^+$ DCs into Tumors

(A) Scheme of TLR3 adjuvant therapy in EG7-bearing congenic mice. C57BL/6(CD45.1) mice were inoculated with EG7 ($CD45.2^+$ lymphoma) cells and treated with PBS (n = 3), poly(I:C)+OVA (n = 4), or ARNAX+OVA (n = 4) on day 7. Tumor growth is shown on the right.

(B) Tumors were harvested on day 12 and single cell suspensions prepared for each sample. Cells were mixed in each group and subjected to flow cytometry. Left: flow cytogram of $CD8^+$ T, NKT, and NK cell populations gated on $CD45.1^+$ cells. Right: proportion of each lymphocyte population in tumor-infiltrating $CD45.1^+$ cells.

(C) Left: flow cytogram of $CD8\alpha^+$ DC population gated on conventional DCs (cDCs). Right: proportion of the DC subset in tumor-infiltrating $CD45.1^+$ cells or cDCs.

(D) Left: flow cytogram of $CD11b^+Ly6G^+$, $CD11b^+Ly6C^+$, and macrophage population gated on $CD45.1^+$ cells. Right: proportion of each myeloid cell population in tumor-infiltrating $CD45.1^+$ cells. Numerical values represent the percentage of gated cells.

See also Figure S6.

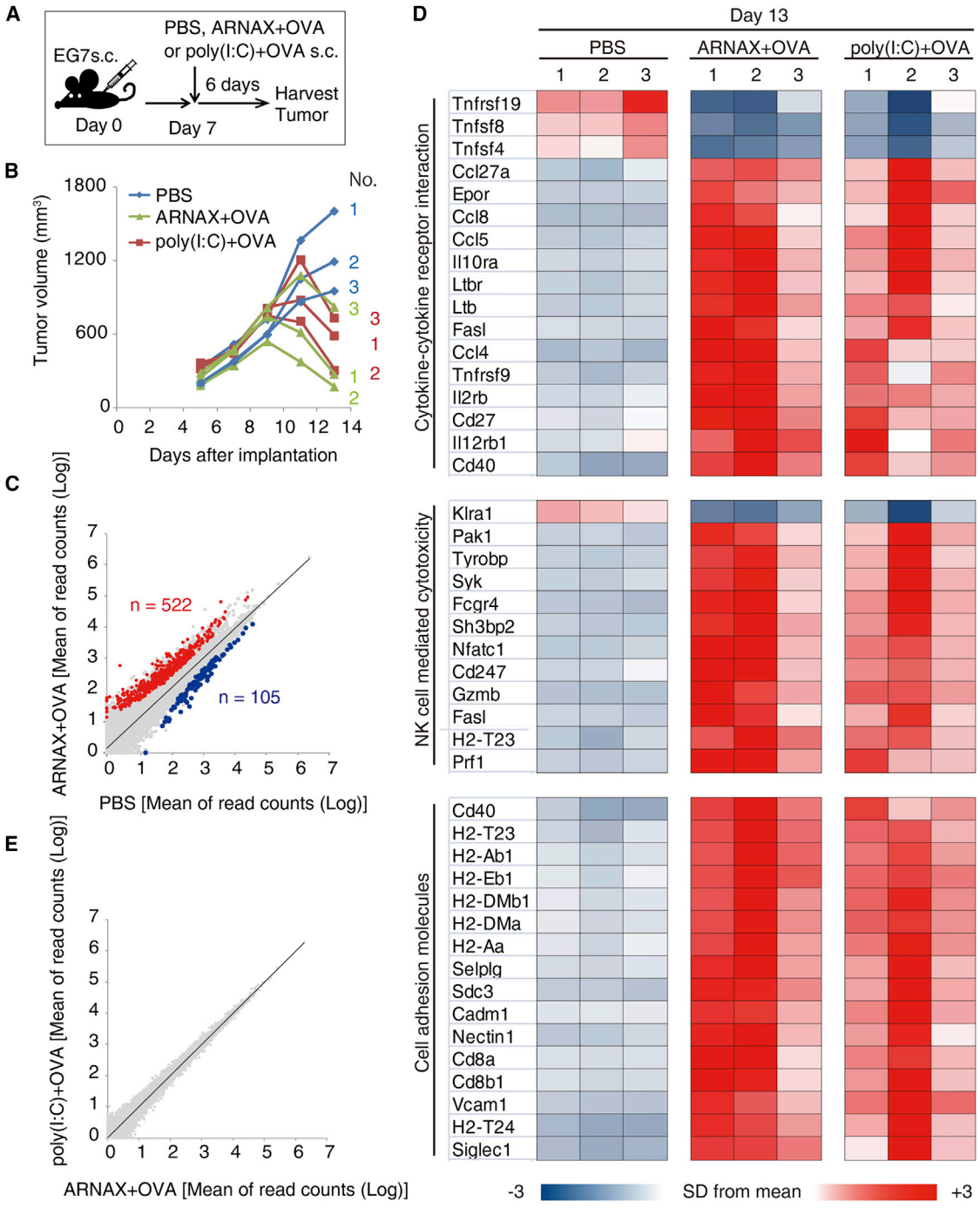

Figure 6. ARNAX Promotes Th1-type Anti-tumor Immunity

(A) EG7-bearing mice were treated with PBS, poly(I:C)+OVA or ARNAX+OVA on day 7. Tumors were harvested on day 13 (n = 3 per group).

(B) Tumor growth of each mouse.

(C) Gene expression (log_{10} normalized read count) in tumors harvested from PBS- or ARNAX+OVA-treated mice on day 13; diagonal line indicates change in expression of 1-fold. Colors indicate significant (adjusted p value, <0.05) upregulation (red; n = 522) or downregulation (blue; n = 105) of expression.

(D) Heatmap illustrating the relative expression patterns of genes in whole tumors from EG7-bearing mice treated with PBS, ARNAX+OVA, or poly(I:C)+OVA on day 13.

(E) Gene expression (log_{10} normalized read count) in tumors harvested from ARNAX+OVA- or poly(I:C)+OVA-treated mice on day 13. Diagonal line indicates change in expression of 1-fold.

See also Figure S7.

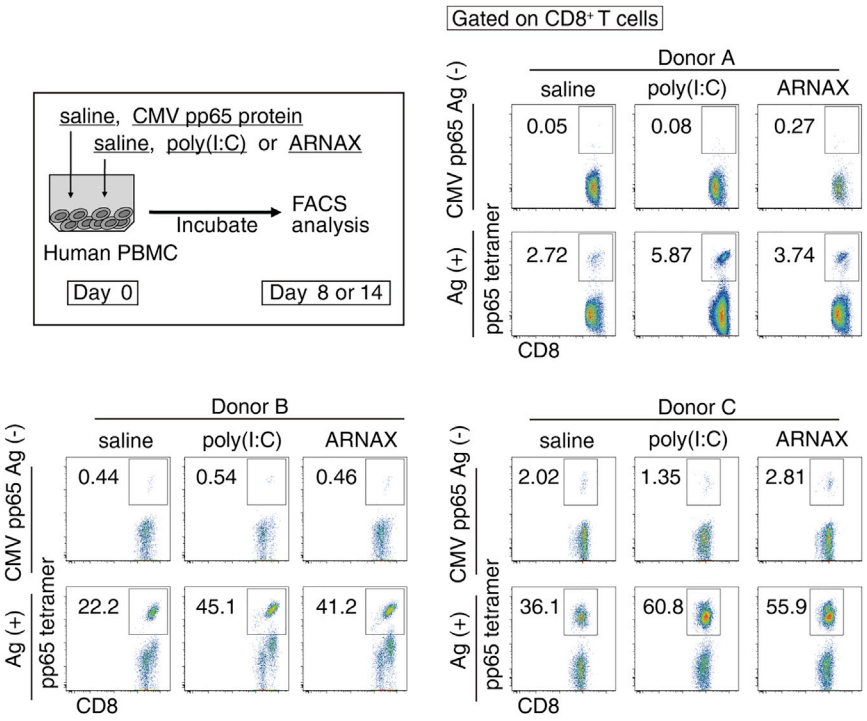

Figure 7. ARNAX Induces Ag-Specific CD8$^+$ T Cells in Human PBMCs

Human PBMCs from healthy donors were stimulated with saline, 20 μg/mL poly(I:C), or ARNAX with or without CMV pp65 recombinant protein and cultured for 8–14 days. Proliferation of CMV pp65-specific CD8$^+$ T cells was evaluated with the tetramer assay and analyzed on FACSAria II. The numerical value in each panel indicates the percentage of CMV pp65 tetramer$^+$ cells in CD8$^+$ T cells.

or control WT1 peptide (Db126: RMFPNAPYL) and IFN-γ production was analyzed with the cytometric bead array (CBA).

In Vivo Mouse Cytokine Assay

Female C57BL/6 mice 7–8 weeks of age were injected s.c. with 200 μL of 150 μg poly(I:C) or ARNAX or intravenously (i.v.) with 200 μL of 50 μg poly(I:C) or ARNAX, and blood was collected from the tail veins at the indicated times. Saline (200 μL) was used as a control. Cytokine levels in sera were measured using CBA. IFN-β and IP-10 levels were quantified with ELISA.

Tumor Challenge and ARNAX Therapy

Female C57BL/6 mice 7 weeks of age were injected s.c. with 200 μL of 2 × 10^6 wild-type EG7, PD-L1^{lo}EG7, or PD-L1^{hi}EG7 cells in PBS (−). Tumor volumes were measured at regular intervals using a caliper and calculated by the following formula: tumor volume (mm^3) = (long diameter) × (short diameter)^2 × 0.52. When the average tumor volume reached ~600 mm^3 (day 7), 100 μL of 100 μg EndoOVA in PBS (−) with or without 100 μL of 60 μg poly(I:C) or ARNAX was injected s.c. around the tumor. PBS (−) (200 μL) was used as a control. On day 13 or 14, spleens and tumors were excised from tumor-bearing mice and further analyzed. For PD-L1 blockade, tumor-bearing mice were injected i.p. with 200 μg anti-mouse PD-L1 monoclonal antibody (mAb) (10F.9G2; Bio X Cell) or rat IgG$_2$b isotype control (LTF-2; Bio X Cell) on days 5, 7, 9, and 11.

Analysis of EG7 Tumors

For confocal microscopy, 4% paraformaldehyde-fixed frozen tumor sections were stained with APC-anti-mouse CD8α mAb and DAPI and analyzed under a LSM510 META microscope (Zeiss). The number of CD8$^+$ cells infiltrating tumors was counted from randomly selected fields (0.2 mm^2 per field). Tumors were finely minced and treated with 25 μg/mL collagenase I (Sigma-Aldrich), collagenase IV (Sigma-Aldrich), 12.5 μg/mL hyaluronidase (Sigma-Aldrich), and 5 μg/mL DNase I (Roche) in Hanks' balanced salt solution (Sigma-Aldrich) at 33°C for 15 min for flow cytometry analysis. Red blood cells were lysed with ACK lysis buffer. Cells were stained with antibodies and analyzed on FACSAria II (BD Biosciences). Data analysis was performed with FlowJo software (Tree Star). The gating strategies are presented in Figure S6. For analysis of gene expression in tumors, total RNA was extracted using TRIzol reagent (QIAGEN) with a high capacity cDNA Reverse Transcription kit (Applied Biosystems) and random primers, according to the manufacturer's instructions. qPCR was performed using specific primers (Table S2) and the Step One Real-time PCR system (Applied Biosystems).

RNA-Seq Analysis

EG7-implanted mice were treated with PBS, poly(I:C)+OVA or ARNAX+OVA on day 7. Tumor tissues harvested on day 8 or 13 were homogenized in TRIzol regent and total RNA was extracted according to the manufacturer's instructions. Bioanalyzer (Agilent) was used to validate quality and quantity of purified RNA. Library construction for RNA-seq was performed with the TruSeq Stranded mRNA LT Sample Prep Kit (Illumina) according to the manufacturer's instructions, and the product was subjected to Hiseq 2500 with the 100 bp single-end protocol (Illumina). Acquired reads were mapped on mouse genome GRCm38 by Tophat2 v2.1.1 (Kim et al., 2013), with the annotation described in gtf release-85 allowing multiple hits up to 100. Multiple mapped reads were segregated and distributed in a random manner using an in-house script. Reads on protein coding genes were counted using HTSeq (Anders et al., 2015) with the gtf using only the protein-coding feature. Differentially expressed genes were examined by DESeq (Anders and Huber, 2010). Genes of interest on pathways annotated in KEGG were selected in cases where expression levels were significantly different (adjusted p value <0.05 and ±2-fold) among ARNX+OVA (day 13) and PBS (day 13) groups. Read counts were normalized by total mapped reads and fit on standard normal distribution to depict heatmaps.

Induction of CMV-Specific CD8$^+$ T Cells in Human PBMCs

Human PBMCs were isolated from the peripheral blood of healthy donors with informed consent. The protocol was approved by the Ethical Committee of Hokkaido University Graduate School of Medicine. Cells (0.5–1 × 10^7/mL) were suspended in RPMI1640 supplemented with 5% auto-plasma, 55 μM 2-ME, and 50 IU penicillin/50 μg/mL streptomycin and stimulated with saline, 20 μg/mL poly(I:C), or ARNAX with or without HCMV pp65 recombinant protein on a 96-well plate. At 48 hr after culture, equal volumes of medium containing recombinant human IL-2 (100 U/mL) were added to the wells and further cultured for 8–14 days. Half of the medium was exchanged with fresh medium containing 50 U/mL hIL-2 twice a week. Proliferation of CMV pp65-specific CD8$^+$ T cells was measured with HLA-A*02:01 or HLA-A*24:02 CMV pp65 tetramer according to the manufacturer's instructions (MBL) and analyzed on FACSAria II. Human data were anonymized employing the methods for the protection of personal information recommended by the Ministry of Health, Labor and Welfare, Japan.

Statistical Analysis

The significance of differences between two groups was determined with the Student's t test. Kruskal-Wallis test with Dunn's multiple comparison was

performed for more than two groups. Error bars represent SD or SEM between samples.

ACCESSION NUMBERS

The accession number for the RNA-seq data reported in this paper is DNA Data Bank of Japan (DDBJ): DRA005314-005319.

SUPPLEMENTAL INFORMATION

Supplemental Information includes seven figures and two tables can be found with this article online at http://dx.doi.org/10.1016/j.celrep.2017.05.015.

AUTHOR CONTRIBUTIONS

Y.T., T.S., and M.M. conceived and designed the experiments. Y.T. performed most of the tumor experiments. K.K. established PD-L1-expressing tumor cell lines. J.Y. performed RNA-sequencing and informatics data analysis. Y.T., K.K., S.O., T.S., and M.M. analyzed the data. K.K. and S.O. provided the materials. Y.T., T.S., and M.M. wrote the paper.

ACKNOWLEDGMENTS

We are grateful to Drs. H. Shime, H. Takaki, K. Funami, M. Tatematsu, and K. Takashima in our laboratory for invaluable discussions; Dr. H. Oshiumi (Kumamoto University) for preparation of KO mice; Ms. F. Nishikawa (NAIST) for suggestion of ARNAX synthesis; Drs. H. Udono (Okayama University) and H. Sugiyama (Osaka University) for providing the tumor cell lines; and Drs. S. Akira (Osaka University) and T. Taniguchi (University of Tokyo) for knockout mice. Thanks are also due to Drs. H. Kida, Y. Suzuki, C. Sugimoto, Mses. N. Kawai, A. Ohnuma (Research Center for Zoonosis Control, Hokkaido University), and Dr. I. Sugimura (Institute for the Promotion of Business-Regional Collaboration, Hokkaido University) for their support of RNA-seq analysis and to Drs. M. Kasahara (Hokkaido University), M. Fukushima, and H. Nishimura (Translational Research Informatics Center, Kobe) for their support of our study. Technical assistance by Ms. Noriko Ishii-Mugikura and Ms. Akiko Morii-Sakai in our laboratory is gratefully acknowledged. This work was supported in part by Grants-in-Aid from the Drug Discovery Support Promotion Project from Japan Agency for Medical Research and Development (AMED) (16nk0101327h0002), by the Akiyama Life Science Foundation, and the Uehara Memorial Foundation.

Received: January 11, 2017
Revised: March 30, 2017
Accepted: May 3, 2017
Published: May 30, 2017

REFERENCES

Anders, S., and Huber, W. (2010). Differential expression analysis for sequence count data. Genome Biol. *11*, R106.

Anders, S., Pyl, P.T., and Huber, W. (2015). HTSeq–a Python framework to work with high-throughput sequencing data. Bioinformatics *31*, 166–169.

Azuma, M., Ebihara, T., Oshiumi, H., Matsumoto, M., and Seya, T. (2012). Cross-priming for antitumor CTL induced by soluble Ag + polyI:C depends on the TICAM-1 pathway in mouse CD11c(+)/CD8α(+) dendritic cells. OncoImmunology *1*, 581–592.

Azuma, M., Takeda, Y., Nakajima, H., Sugiyama, H., Ebihara, T., Oshiumi, H., Matsumoto, M., and Seya, T. (2016). Biphasic function of TLR3 adjuvant on tumor and spleen dendritic cells promotes tumor T cell infiltration and regression in a vaccine therapy. OncoImmunology *5*, e1188244.

Bachem, A., Güttler, S., Hartung, E., Ebstein, F., Schaefer, M., Tannert, A., Salama, A., Movassaghi, K., Opitz, C., Mages, H.W., et al. (2010). Superior antigen cross-presentation and XCR1 expression define human CD11c+CD141+ cells as homologues of mouse CD8+ dendritic cells. J. Exp. Med. *207*, 1273–1281.

Bachmann, M.F., Kopf, M., and Marsland, B.J. (2006). Chemokines: more than just road signs. Nat. Rev. Immunol. *6*, 159–164.

Coulie, P.G., Van den Eynde, B.J., van der Bruggen, P., and Boon, T. (2014). Tumour antigens recognized by T lymphocytes: at the core of cancer immunotherapy. Nat. Rev. Cancer *14*, 135–146.

Coussens, L.M., Zitvogel, L., and Palucka, A.K. (2013). Neutralizing tumor-promoting chronic inflammation: a magic bullet? Science *339*, 286–291.

Curiel, T.J., Wei, S., Dong, H., Alvarez, X., Cheng, P., Mottram, P., Krzysiek, R., Knutson, K.L., Daniel, B., Zimmermann, M.C., et al. (2003). Blockade of B7-H1 improves myeloid dendritic cell-mediated antitumor immunity. Nat. Med. *9*, 562–567.

Curtsinger, J.M., and Mescher, M.F. (2010). Inflammatory cytokines as a third signal for T cell activation. Curr. Opin. Immunol. *22*, 333–340.

De Henau, O., Rausch, M., Winkler, D., Campesato, L.F., Liu, C., Cymerman, D.H., Budhu, S., Ghosh, A., Pink, M., Tchaicha, J., et al. (2016). Overcoming resistance to checkpoint blockade therapy by targeting PI3Kγ in myeloid cells. Nature *539*, 443–447.

Eisenbarth, S.C., Colegio, O.R., O'Connor, W., Sutterwala, F.S., and Flavell, R.A. (2008). Crucial role for the Nalp3 inflammasome in the immunostimulatory properties of aluminium adjuvants. Nature *453*, 1122–1126.

Fuertes, M.B., Kacha, A.K., Kline, J., Woo, S.R., Kranz, D.M., Murphy, K.M., and Gajewski, T.F. (2011). Host type I IFN signals are required for antitumor CD8+ T cell responses through CD8α+ dendritic cells. J. Exp. Med. *208*, 2005–2016.

Fuertes, M.B., Woo, S.R., Burnett, B., Fu, Y.X., and Gajewski, T.F. (2013). Type I interferon response and innate immune sensing of cancer. Trends Immunol. *34*, 67–73.

Gajewski, T.F., Woo, S.R., Zha, Y., Spaapen, R., Zheng, Y., Corrales, L., and Spranger, S. (2013). Cancer immunotherapy strategies based on overcoming barriers within the tumor microenvironment. Curr. Opin. Immunol. *25*, 268–276.

Galluzzi, L., Vacchelli, E., Eggermont, A., Fridman, W.H., Galon, J., Sautès-Fridman, C., Tartour, E., Zitvogel, L., and Kroemer, G. (2012). Trial watch: experimental Toll-like receptor agonists for cancer therapy. OncoImmunology *1*, 699–716.

Gerner, M.Y., Heltemes-Harris, L.M., Fife, B.T., and Mescher, M.F. (2013). Cutting edge: IL-12 and type I IFN differentially program CD8 T cells for programmed death 1 re-expression levels and tumor control. J. Immunol. *191*, 1011–1015.

Hamid, O., Robert, C., Daud, A., Hodi, F.S., Hwu, W.-J., Kefford, R., Wolchok, J.D., Hersey, P., Joseph, R.W., Weber, J.S., et al. (2013). Safety and tumor responses with lambrolizumab (anti-PD-1) in melanoma. N. Engl. J. Med. *369*, 134–144.

Herbst, R.S., Soria, J.C., Kowanetz, M., Fine, G.D., Hamid, O., Gordon, M.S., Sosman, J.A., McDermott, D.F., Powderly, J.D., Gettinger, S.N., et al. (2014). Predictive correlates of response to the anti-PD-L1 antibody MPDL3280A in cancer patients. Nature *515*, 563–567.

Hugo, W., Zaretsky, J.M., Sun, L., Song, C., Moreno, B.H., Hu-Lieskovan, S., Berent-Maoz, B., Pang, J., Chmielowski, B., Cherry, G., et al. (2016). Genomic and transcriptomic features of response to anti-PD-1 therapy in metastatic melanoma. Cell *165*, 35–44.

Jongbloed, S.L., Kassianos, A.J., McDonald, K.J., Clark, G.J., Ju, X., Angel, C.E., Chen, C.J., Dunbar, P.R., Wadley, R.B., Jeet, V., et al. (2010). Human CD141+ (BDCA-3)+ dendritic cells (DCs) represent a unique myeloid DC subset that cross-presents necrotic cell antigens. J. Exp. Med. *207*, 1247–1260.

Joyce, J.A., and Fearon, D.T. (2015). T cell exclusion, immune privilege, and the tumor microenvironment. Science *348*, 74–80.

Kaech, S.M., and Cui, W. (2012). Transcriptional control of effector and memory CD8+ T cell differentiation. Nat. Rev. Immunol. *12*, 749–761.

Kamphorst, A.O., and Ahmed, R. (2013). Manipulating the PD-1 pathway to improve immunity. Curr. Opin. Immunol. *25*, 381–388.

Kataoka, K., Shiraishi, Y., Takeda, Y., Sakata, S., Matsumoto, M., Nagano, S., Maeda, T., Nagata, Y., Kitanaka, A., Mizuno, S., et al. (2016). Aberrant PD-L1

expression through 3′-UTR disruption in multiple cancers. Nature *534*, 402–406.

Kato, H., Takeuchi, O., Sato, S., Yoneyama, M., Yamamoto, M., Matsui, K., Uematsu, S., Jung, A., Kawai, T., Ishii, K.J., et al. (2006). Differential roles of MDA5 and RIG-I helicases in the recognition of RNA viruses. Nature *441*, 101–105.

Keir, M.E., Butte, M.J., Freeman, G.J., and Sharpe, A.H. (2008). PD-1 and its ligands in tolerance and immunity. Annu. Rev. Immunol. *26*, 677–704.

Kim, D., Pertea, G., Trapnell, C., Pimentel, H., Kelley, R., and Salzberg, S.L. (2013). TopHat2: accurate alignment of transcriptomes in the presence of insertions, deletions and gene fusions. Genome Biol. *14*, R36.

Kroemer, G., Galluzzi, L., Kepp, O., and Zitvogel, L. (2013). Immunogenic cell death in cancer therapy. Annu. Rev. Immunol. *31*, 51–72.

Lampkin, B.C., Levine, A.S., Levy, H., Krivit, W., and Hammond, D. (1985). Phase II trial of a complex polyriboinosinic-polyribocytidylic acid with poly-L-lysine and carboxymethyl cellulose in the treatment of children with acute leukemia and neuroblastoma: a report from the Children's Cancer Study Group. Cancer Res. *45*, 5904–5909.

Levine, A.S., Sivulich, M., Wiernik, P.H., and Levy, H.B. (1979). Initial clinical trials in cancer patients of polyriboinosinic-polyribocytidylic acid stabilized with poly-L-lysine, in carboxymethylcellulose [poly(ICLC)], a highly effective interferon inducer. Cancer Res. *39*, 1645–1650.

Mantovani, A., Allavena, P., Sica, A., and Balkwill, F. (2008). Cancer-related inflammation. Nature *454*, 436–444.

Matsumoto, M., and Seya, T. (2008). TLR3: interferon induction by double-stranded RNA including poly(I:C). Adv. Drug Deliv. Rev. *60*, 805–812.

Matsumoto, M., Tatematsu, M., Nishikawa, F., Azuma, M., Ishii, N., Morii-Sakai, A., Shime, H., and Seya, T. (2015). Defined TLR3-specific adjuvant that induces NK and CTL activation without significant cytokine production in vivo. Nat. Commun. *6*, 6280.

Mbow, M.L., De Gregorio, E., Valiante, N.M., and Rappuoli, R. (2010). New adjuvants for human vaccines. Curr. Opin. Immunol. *22*, 411–416.

Pantel, A., Teixeira, A., Haddad, E., Wood, E.G., Steinman, R.M., and Longhi, M.P. (2014). Direct type I IFN but not MDA5/TLR3 activation of dendritic cells is required for maturation and metabolic shift to glycolysis after poly IC stimulation. PLoS Biol. *12*, e1001759.

Peranzoni, E., Zilio, S., Marigo, I., Dolcetti, L., Zanovello, P., Mandruzzato, S., and Bronte, V. (2010). Myeloid-derived suppressor cell heterogeneity and subset definition. Curr. Opin. Immunol. *22*, 238–244.

Rizvi, N.A., Hellmann, M.D., Snyder, A., Kvistborg, P., Makarov, V., Havel, J.J., Lee, W., Yuan, J., Wong, P., Ho, T.S., et al. (2015). Cancer immunology. Mutational landscape determines sensitivity to PD-1 blockade in non-small cell lung cancer. Science *348*, 124–128.

Ryu, M.S., Woo, M.Y., Kwon, D., Hong, A.E., Song, K.Y., Park, S., and Lim, I.K. (2014). Accumulation of cytolytic $CD8^+$ T cells in B16-melanoma and proliferation of mature T cells in TIS21-knockout mice after T cell receptor stimulation. Exp. Cell Res. *327*, 209–221.

Sabbatini, P., Tsuji, T., Ferran, L., Ritter, E., Sedrak, C., Tuballes, K., Jungbluth, A.A., Ritter, G., Aghajanian, C., Bell-McGuinn, K., et al. (2012). Phase I trial of overlapping long peptides from a tumor self-antigen and poly-ICLC shows rapid induction of integrated immune response in ovarian cancer patients. Clin. Cancer Res. *18*, 6497–6508.

Salmon, H., Idoyaga, J., Rahman, A., Leboeuf, M., Remark, R., Jordan, S., Casanova-Acebes, M., Khudoynazarova, M., Agudo, J., Tung, N., et al. (2016). Expansion and activation of CD103(+) dendritic cell progenitors at the tumor site enhances tumor responses to therapeutic PD-L1 and BRAF inhibition. Immunity *44*, 924–938.

Schietinger, A., and Greenberg, P.D. (2014). Tolerance and exhaustion: defining mechanisms of T cell dysfunction. Trends Immunol. *35*, 51–60.

Schumacher, T.N., and Schreiber, R.D. (2015). Neoantigens in cancer immunotherapy. Science *348*, 69–74.

Seya, T., and Matsumoto, M. (2009). The extrinsic RNA-sensing pathway for adjuvant immunotherapy of cancer. Cancer Immunol. Immunother. *58*, 1175–1184.

Seya, T., Takeda, Y., and Matsumoto, M. (2015). Tumor vaccines with dsRNA adjuvant ARNAX induces antigen-specific tumor shrinkage without cytokinemia. OncoImmunology *5*, e1043506.

Sharma, P., and Allison, J.P. (2015a). Immune checkpoint targeting in cancer therapy: toward combination strategies with curative potential. Cell *161*, 205–214.

Sharma, P., and Allison, J.P. (2015b). The future of immune checkpoint therapy. Science *348*, 56–61.

Shime, H., Matsumoto, M., Oshiumi, H., Tanaka, S., Nakane, A., Iwakura, Y., Tahara, H., Inoue, N., and Seya, T. (2012). Toll-like receptor 3 signaling converts tumor-supporting myeloid cells to tumoricidal effectors. Proc. Natl. Acad. Sci. USA *109*, 2066–2071.

Shime, H., Matsumoto, M., and Seya, T. (2017). Double-stranded RNA promotes CTL-independent tumor cytolysis mediated by $CD11b^+Ly6G^+$ intratumor myeloid cells through the TICAM-1 signaling pathway. Cell Death Differ. *24*, 385–396.

Sistigu, A., Yamazaki, T., Vacchelli, E., Chaba, K., Enot, D.P., Adam, J., Vitale, I., Goubar, A., Baracco, E.E., Remédios, C., et al. (2014). Cancer cell-autonomous contribution of type I interferon signaling to the efficacy of chemotherapy. Nat. Med. *20*, 1301–1309.

Steinman, R.M., and Banchereau, J. (2007). Taking dendritic cells into medicine. Nature *449*, 419–426.

Takeda, Y., Azuma, M., Matsumoto, M., and Seya, T. (2016). Tumoricidal efficacy coincides with CD11c up-regulation in antigen-specific CD8(+) T cells during vaccine immunotherapy. J. Exp. Clin. Cancer Res. *35*, 143.

Tumeh, P.C., Harview, C.L., Yearley, J.H., Shintaku, I.P., Taylor, E.J., Robert, L., Chmielowski, B., Spasic, M., Henry, G., Ciobanu, V., et al. (2014). PD-1 blockade induces responses by inhibiting adaptive immune resistance. Nature *515*, 568–571.

Youn, J.I., Nagaraj, S., Collazo, M., and Gabrilovich, D.I. (2008). Subsets of myeloid-derived suppressor cells in tumor-bearing mice. J. Immunol. *181*, 5791–5802.

Zelenay, S., van der Veen, A.G., Böttcher, J.P., Snelgrove, K.J., Rogers, N., Acton, S.E., Chakravarty, P., Girotti, M.R., Marais, R., Quezada, S.A., et al. (2015). Cyclooxygenase-dependent tumor growth through evasion of immunity. Cell *162*, 1257–1270.

Zou, W., Wolchok, J.D., and Chen, L. (2016). PD-L1 (B7-H1) and PD-1 pathway blockade for cancer therapy: Mechanisms, response biomarkers, and combinations. Sci. Transl. Med. *8*, 328rv4.

Cell Reports, Volume *19*

Supplemental Information

A TLR3-Specific Adjuvant Relieves Innate Resistance to PD-L1 Blockade without Cytokine Toxicity in Tumor Vaccine Immunotherapy

Yohei Takeda, Keisuke Kataoka, Junya Yamagishi, Seishi Ogawa, Tsukasa Seya, and Misako Matsumoto

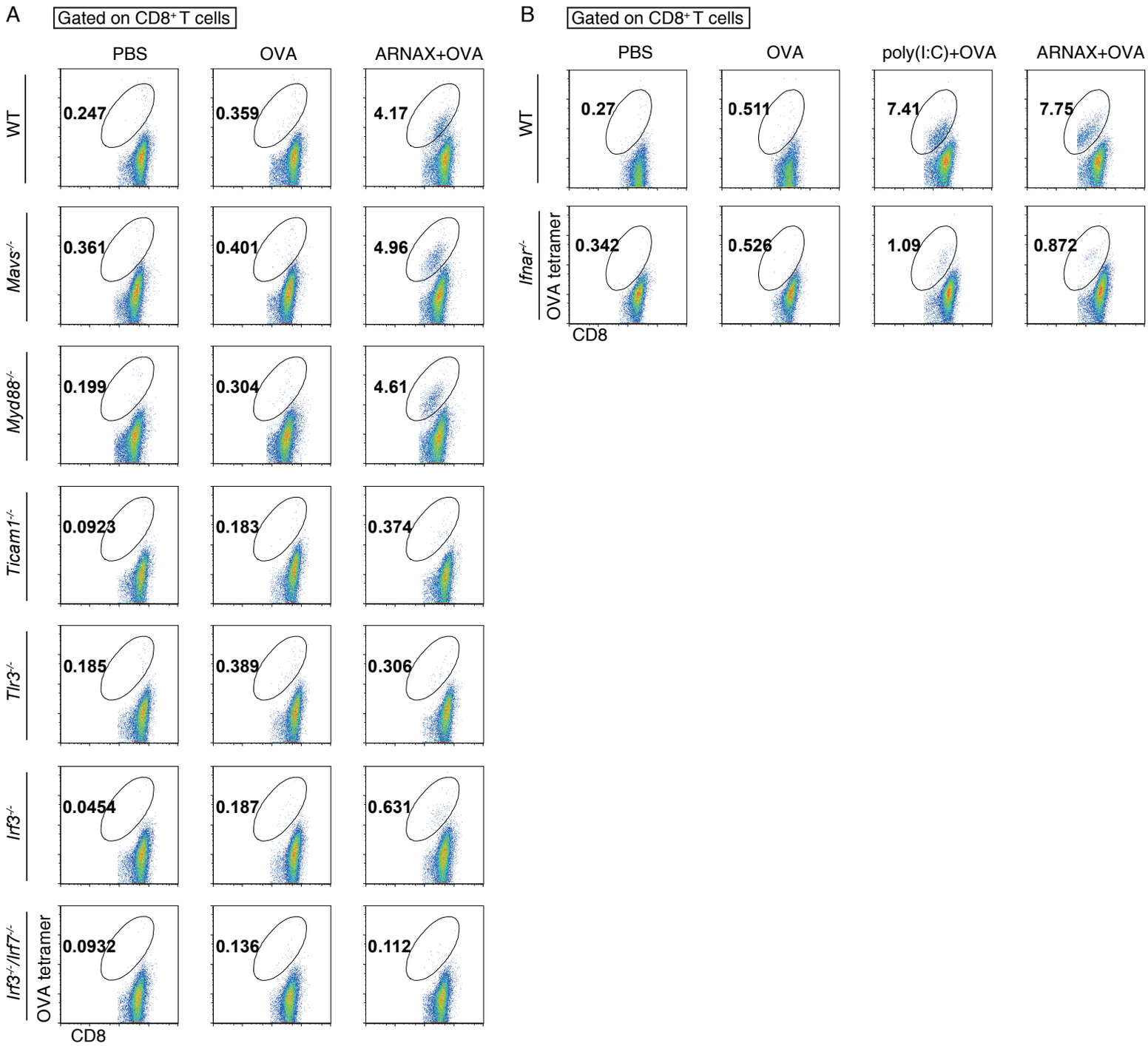

Figure S1. Representative flow cytogram of ARNAX-induced cross-priming in wild-type and knockout mice. Related to Figure 1.
(A, B) Wild-type and indicated knockout mice were injected s.c. with PBS, OVA, ARNAX+OVA or poly(I:C)+OVA twice per week. Spleen and inguinal LNs were harvested 4 days after the last adjuvant injection and stained for CD3, CD8α and OVA tetramer. Representative spleen FACS data from each experiment are shown.

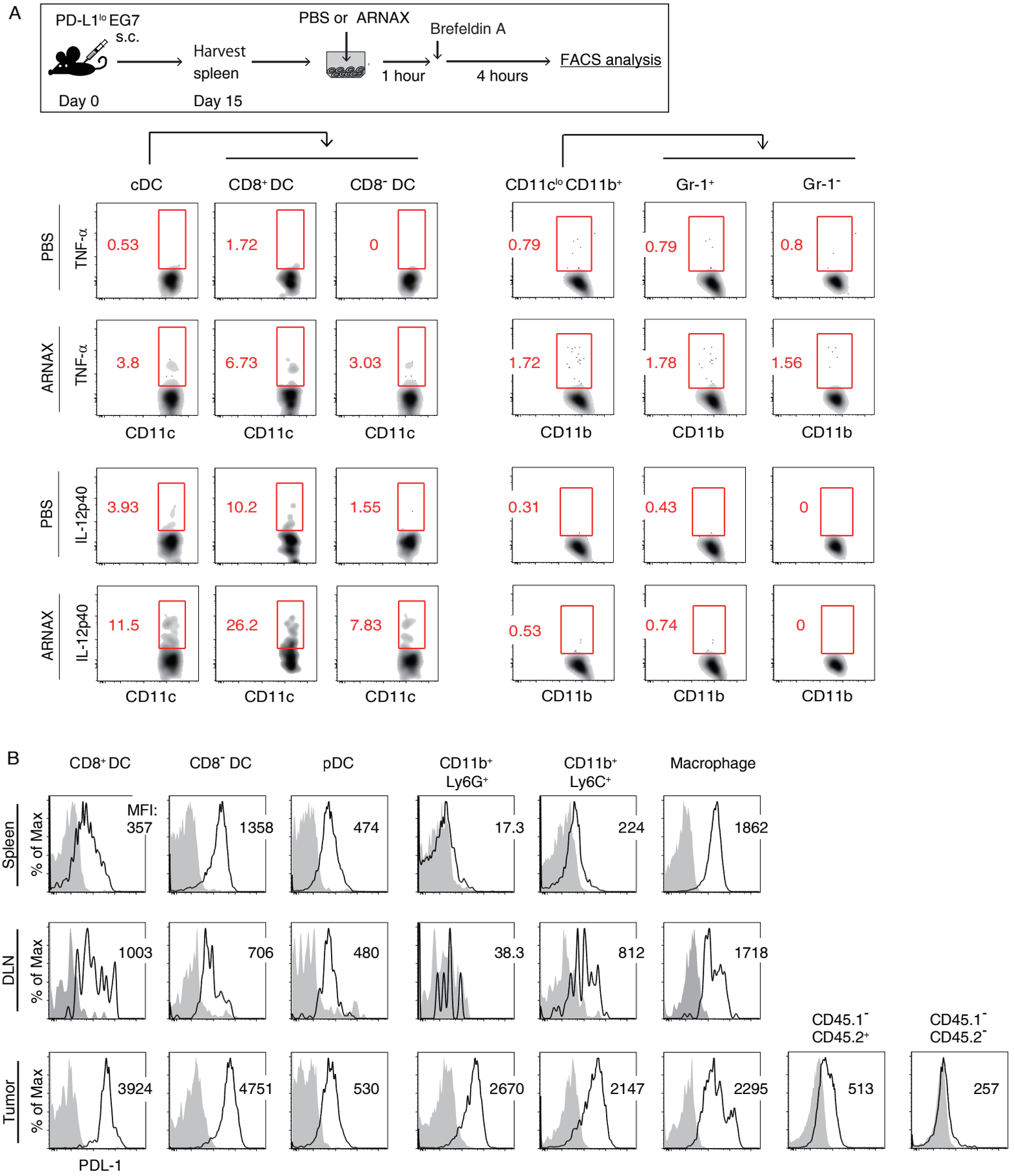

Figure S2. Targets of ARNAX and PD-L1 expression on APCs in EG7-bearing mice. Related to Figures 3 and 4.
(A) Defining *in vivo* targets of ARNAX. Experimental scheme is shown in the upper panel. Spleen cells from PD-L1^{lo} EG7-bearing mice (n=3) were stimulated with PBS or ARNAX (10 μg/ml). Cells responding to ARNAX were independently analyzed in each mouse by intracellular cytokine staining for IL-12p40 and TNF-α using flow cytometry. Representative flow cytogram from three mice data are shown. The numerical value in each panel represents the percentage of TNF-α- or IL-12p40-producing cells in the indicated cell-type. (B) PD-L1 expression on APCs in spleen, DLN and tumor environments in PD-L1^{lo} EG7-bearing mice. C57BL/6 (CD45.1) mice were inoculated with PD-L1^{lo} EG7 (CD45.2) cells. On day 15, spleen, inguinal LN and tumor were harvested and single cell suspensions were prepared. Expression of PD-L1 on DC subsets and CD11b^{+} myeloid cells were analyzed by flow cytometry. Representative FACS data from two independent experiments are shown. PD-L1 expression on tumor cells (CD45.1^{-}CD45.2^{+}) is also shown. The CD45.1^{-}CD45.2^{-} population represents tumor-associated non-lymphoid cells, which barely express PD-L1. Shaded and open histograms represent isotype control and PD-L1 staining, respectively. Numerical values represent mean fluorescent intensity of PD-L1 staining.

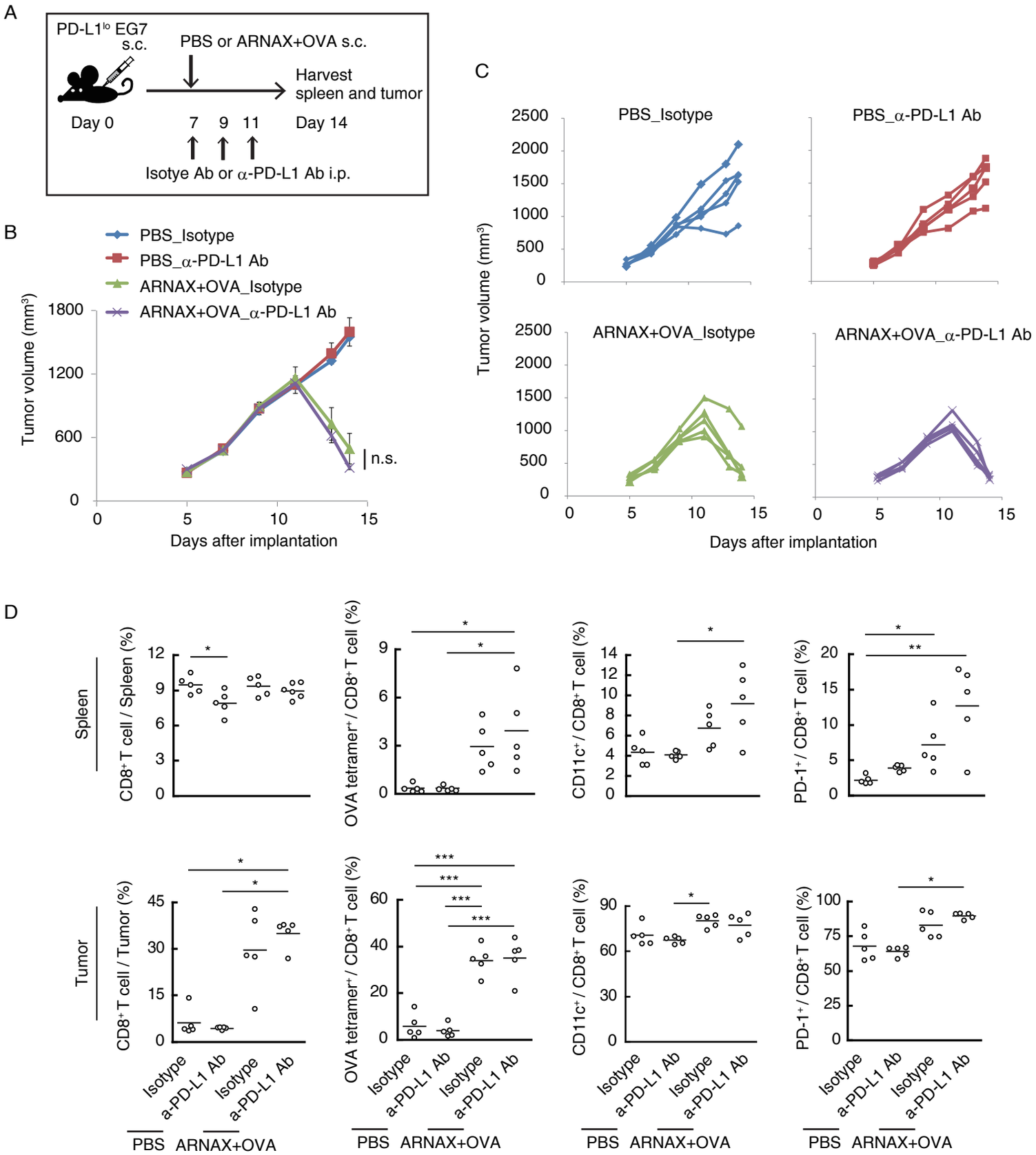

Figure S3. Combination therapy with ARNAX+OVA and anti-PD-L1 Ab in PD-L1^{lo} EG7 tumors. Related to Figure 3.
(A) Scheme of combination therapy of ARNAX+OVA and anti-PD-L1 Ab in PD-L1^{lo} EG7 tumors. (B) PD-L1^{lo} EG7-bearing mice were treated with PBS or ARNAX+OVA in combination with anti-PD-L1 Ab or isotype control Ab as shown in (A), and tumor sizes were evaluated in each group (n=5/group). Error bars indicate means±s.e.m. n.s., not significant with Student's t-test. (C) Tumor growth in individual mice. (D) Spleen and tumors were harvested on day 14 from tumor-bearing mice in each group. CD8$^+$ T cell density, OVA-specific CD8$^+$ T cell proliferation and the proportion of CD8$^+$ T cells expressing CD11c or PD-1 in spleen (upper panels) and intratumors (lower panels) were analyzed via flow cytometry. *p<0.05, **p<0.01, ***p<0.001 by Kruskal-Wallis test with Dunn's multiple comparison test.

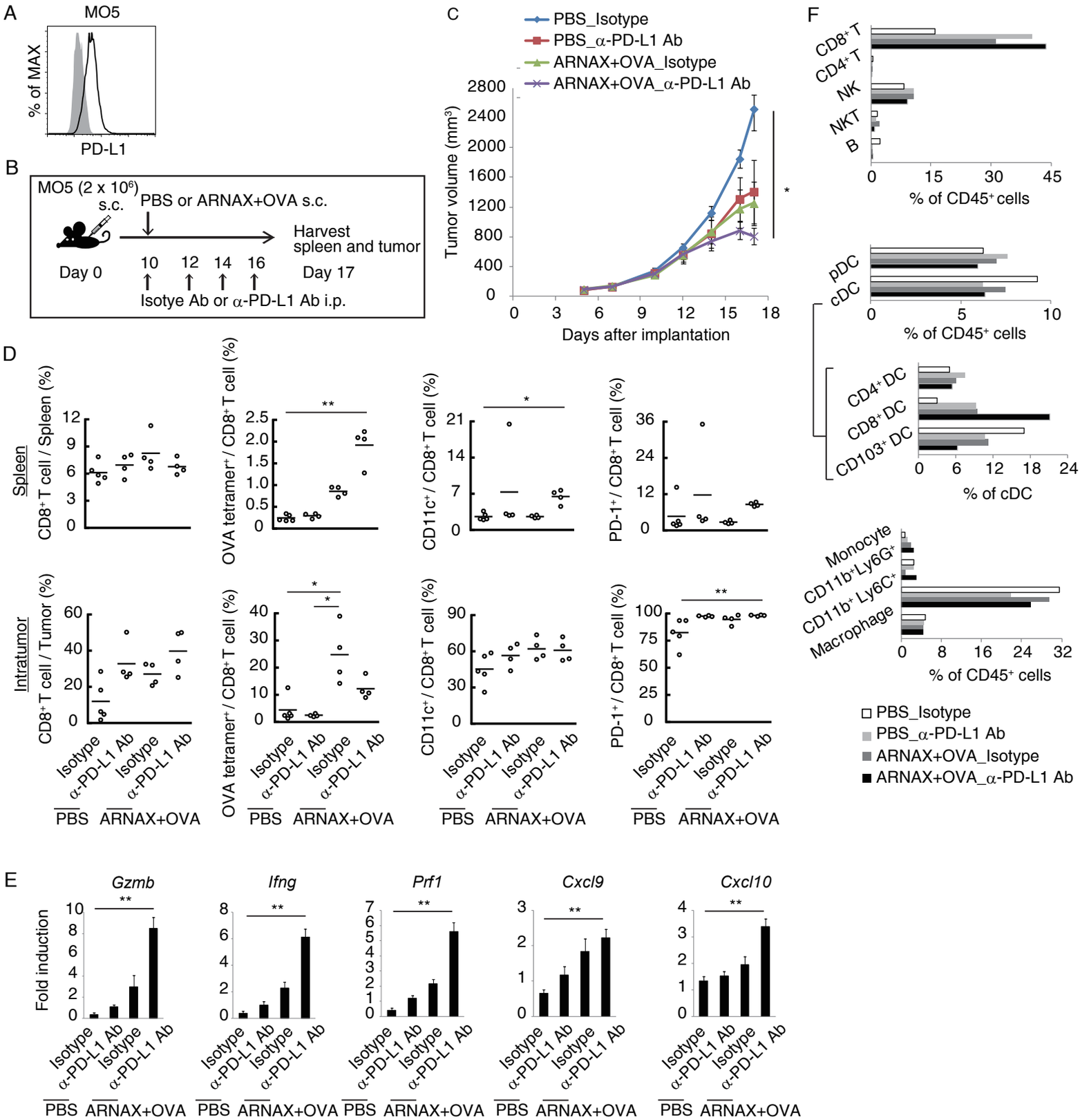

Figure S4. ARNAX+OVA synergistically induce anti-tumor immunity with PD-L1 Ab in MO5 tumors. Related to Figure 4.
(A) PD-L1 expression in MO5 (OVA-expressing B16 melanoma) cells. Shaded and open histograms represent isotype control and PD-L1 staining, respectively. (B) Scheme of combination therapy comprising ARNAX and anti-PD-L1 Ab in MO5 tumors. (C) MO5-bearing mice were treated with PBS or ARNAX+OVA in combination with anti-PD-L1 Ab or isotype control Ab, as shown in (B). Error bars indicate means±s.e.m.: n=4–5 per group. *p<0.05 by Kruskal-Wallis with Dunn's multiple comparison test. (D) Spleens and tumors were harvested on day 17 from tumor-bearing mice in each group. $CD8^+$ T cell density and the proportion of OVA $tetramer^+$, $CD11c^+$ or $PD\text{-}1^+$ $CD8^+$ T cells in spleen (upper panels) and intratumors (lower panels) were analyzed via flow cytometry. (E) Gene expression analysis in tumor-bearing mice on day 17 in each group. *Gzmb*, *Ifng*, *Prf1*, *Cxcl9* and *Cxcl10* mRNA levels were measured using qPCR and normalized to *Gapdh*. Error bars indicate means±s.e.m.; n=4–5 per group. **p<0.01 by Kruskal-Wallis with Dunn's multiple comparison test. (F) Proportion of tumor-infiltrating immune cells. Upper panel, tumor-infiltrating lymphocyte population gated on $CD45^+$ cells. Middle panel, DCs gated on $CD45^+$ cells and each subset gated on cDCs. Lower panel, tumor-infiltrating $CD11b^+$ myeloid cell subset gated on $CD45^+$ cells.

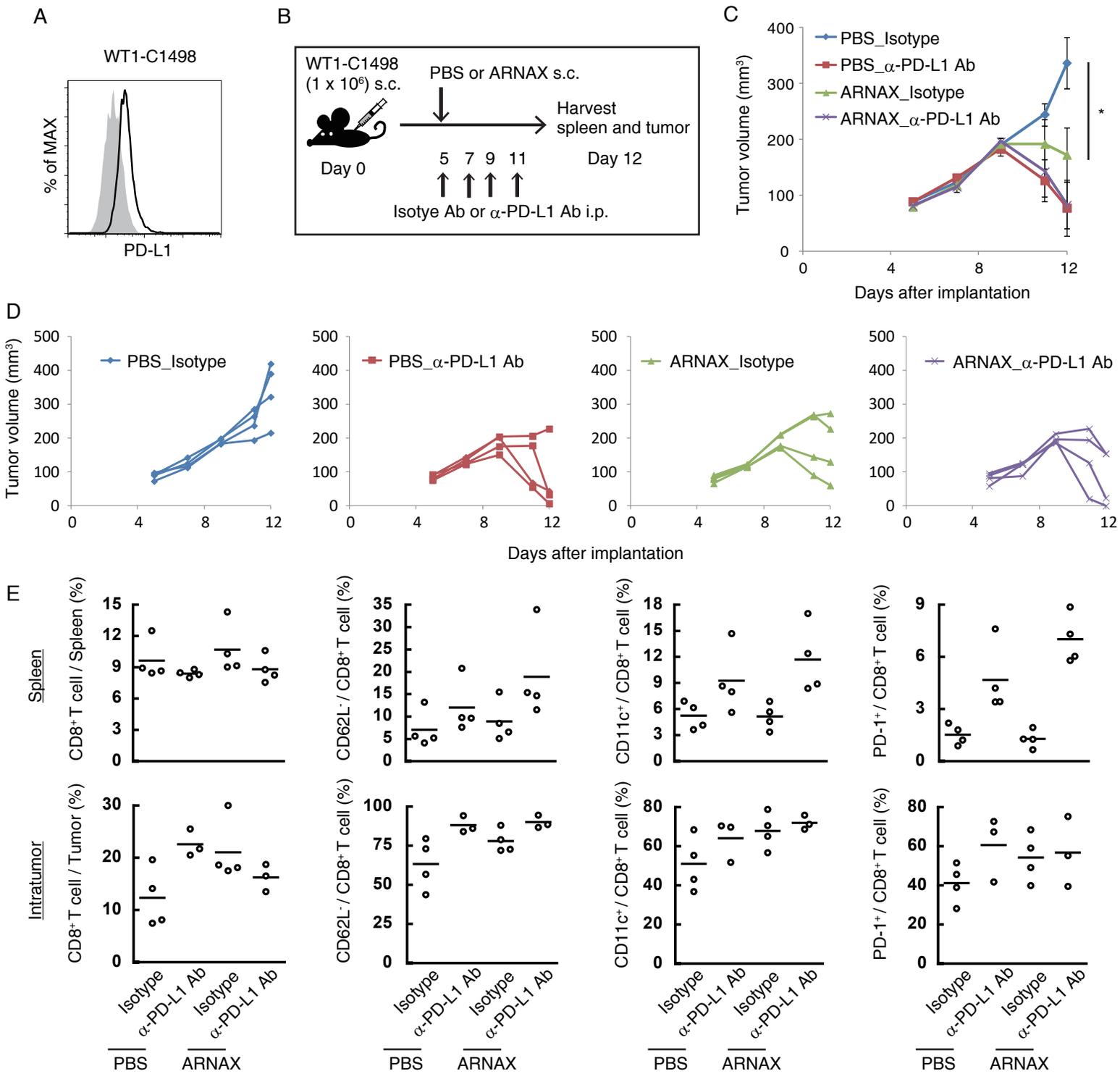

Figure S5. ARNAX induces regression of WT1-C1498 tumors. Related to Figure 4.
(A) PD-L1 expression in WT1-C1498 cells. Shaded and open histograms represent isotype control and PD-L1 staining, respectively. (B) Scheme of combination therapy with ARNAX and anti-PD-L1 Ab in WT1-C1498 tumors. (C) WT1-C1498-bearing mice were treated with PBS or 60 μg ARNAX in combination with anti-PD-L1 Ab or isotype control Ab, as shown in (B). Tumor size was evaluated in each group. Error bars indicate means±s.e.m.: n=4 per group. *$p<0.05$ with Student's t-test. (D) Tumor growth in individual mice. (E) Spleens and tumors were harvested on day 12 from tumor-bearing mice in each group. $CD8^+$ T cell density and the proportion of $CD62L^-$, $CD11c^+$ or $PD\text{-}1^+$ $CD8^+$ T cells in spleen (upper panels) and intratumors (lower panels) were analyzed via flow cytometry.

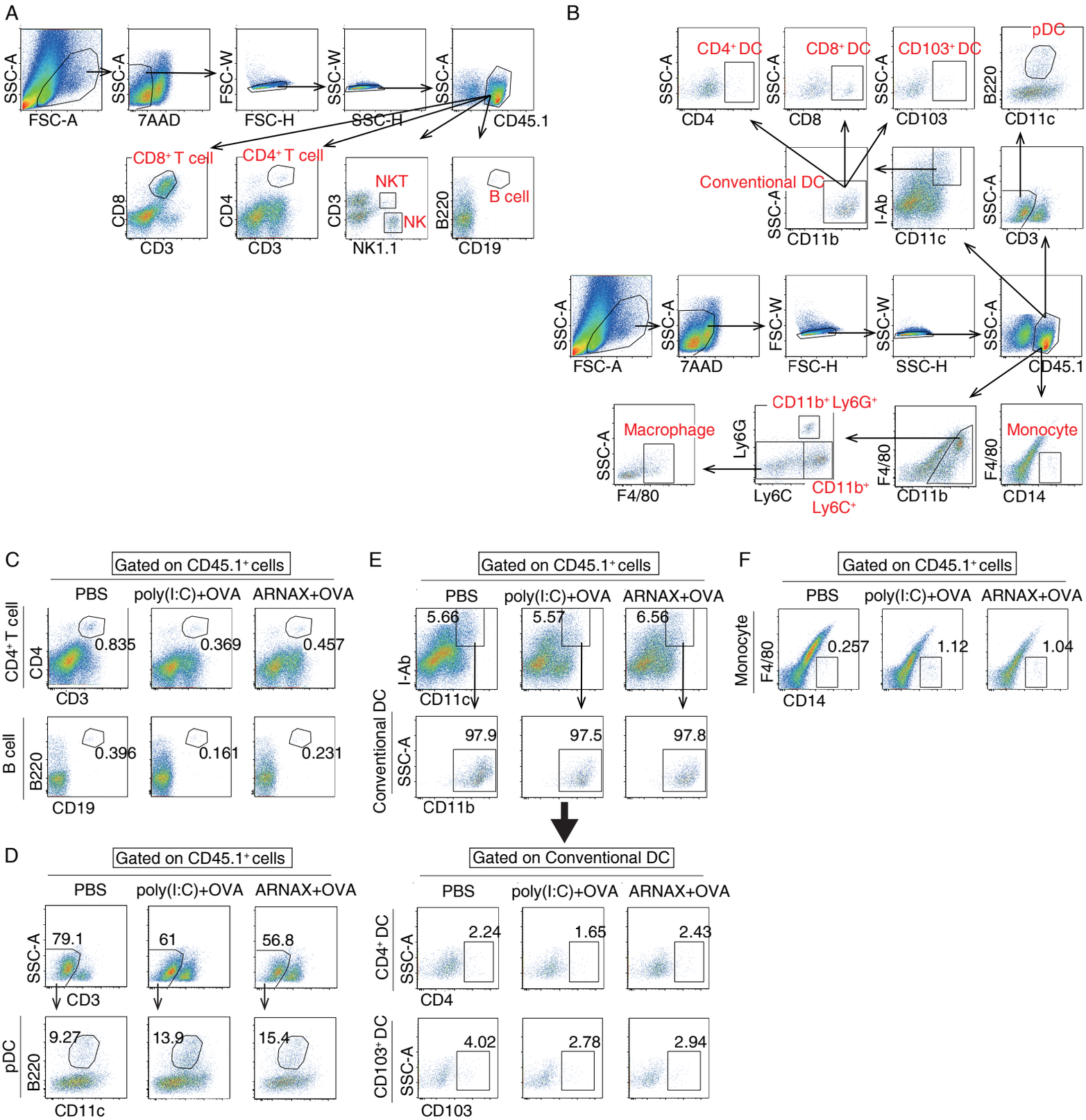

Figure S6. Gating strategy for flow cytometry analysis of tumor-infiltrating immune cells. Related to Figure 5.

(A, B) C57BL/6 (CD45.1) mice were inoculated with EG7 (CD45.2) cells and treated with PBS, poly(I:C)+OVA or ARNAX+OVA on day 7. Tumors were harvested on day 12 and flow cytometry analysis performed using freshly isolated whole tumor cell preparations. CD45.1$^+$ cells were gated, and expression levels of the indicated lymphocyte surface markers (A), DC or myeloid surface markers (B) analyzed.

(C-F) Flow cytogram of CD4$^+$T cells, B cells (C), pDC (D), monocyte (F), cDCs populations gated on CD45.1$^+$ cells and CD4$^+$ DC and CD103$^+$ DCs gated on cDCs (E). Numerical values represent the percentage of gated cells.

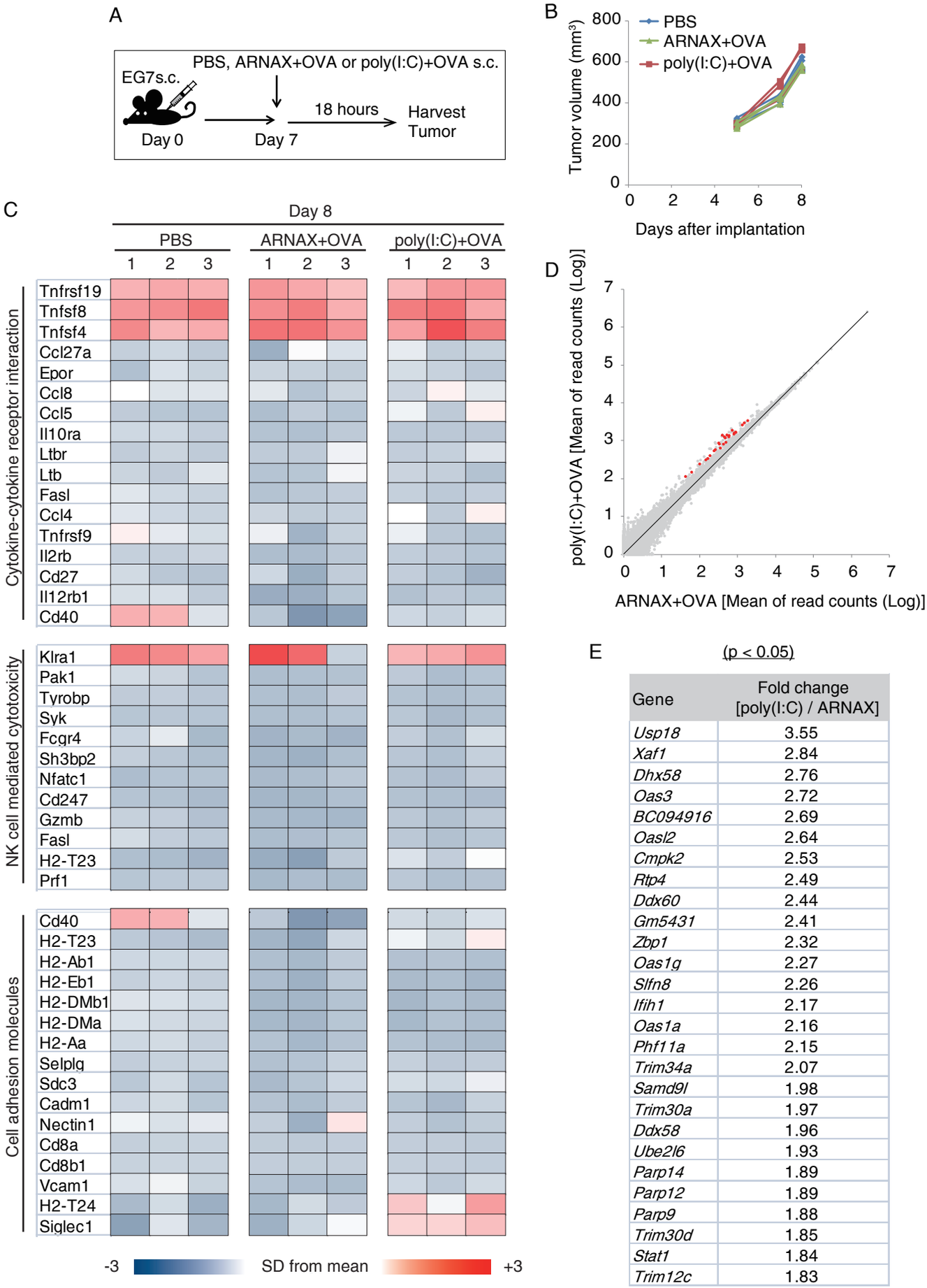

E

(p < 0.05)

Gene	Fold change [poly(I:C) / ARNAX]
Usp18	3.55
Xaf1	2.84
Dhx58	2.76
Oas3	2.72
BC094916	2.69
Oasl2	2.64
Cmpk2	2.53
Rtp4	2.49
Ddx60	2.44
Gm5431	2.41
Zbp1	2.32
Oas1g	2.27
Slfn8	2.26
Ifih1	2.17
Oas1a	2.16
Phf11a	2.15
Trim34a	2.07
Samd9l	1.98
Trim30a	1.97
Ddx58	1.96
Ube2l6	1.93
Parp14	1.89
Parp12	1.89
Parp9	1.88
Trim30d	1.85
Stat1	1.84
Trim12c	1.83

Figure S7. Early tumor responses following ARNAX/poly(I:C)+OVA treatment. Related to Figure 6.
(A) EG7-bearing mice were treated with PBS, ARNAX+OVA or poly(I:C)+OVA on day 7. Tumors were harvested on day 8 (n=3 per group). (B) Tumor growth of each mouse is shown. (C) Heat map illustrating the relative expression of genes in whole tumors from EG7-bearing mice treated with PBS, ARNAX+OVA or poly(I:C)+OVA on day 8. (D) Gene expression (log10 normalized read count) in tumors harvested from ARNAX+OVA- or poly(I:C)+OVA-treated mice on day 8; diagonal line indicates change in expression of 1-fold; red color indicates significant (adjusted p value, <0.05) upregulation of expression. Upregulated gene names and fold changes are shown in (E).

Table S1. Antibodies used for flow cytometry analysis. Related to Figure 1, 3-5, 7, S1, S3-S6.

Antibody	Clone	Supplier
PE-anti-mouse B220 FITC-anti-mouse B220	RA3-6B2	Biolegend
AlxaFluor700-anti-mouse CD3 APC-anti-mouse CD3 FITC-anti-mouse CD3	145-2C11	
PE/Cy7-anti-mouse CD3	17A2	
PE-anti-mouse CD4	GK1.5	
APC-anti-mouse CD8α FITC-anti-mouse CD8α PE-anti-mouse CD8α	53-6.7	
PE/Cy7-anti-mouse CD11b FITC-anti-mouse CD11b	M1/70	
PE/Cy7-anti-mouse CD11c	N418	
Anti-mouse CD16/32	93	
APC-anti-mouse CD19	6D5	
AlxaFluor700-anti-mouse CD45.1	A20	
APC-anti-mouse CD45.2	104	
FITC-labeled anti-mouse CD62L	MEL-14	
PE-anti-mouse CD103	2E7	
APC-anti-mouse F4/80 FITC-anti-mouse F4/80	BM8	
APC-anti-mouse Gr-1	RB6-8C5	
FITC-anti-mouse I-Ab	KH74	
PE-anti-mouse IL-12p40	C15.6	
APC-anti-mouse Ly-6C FITC-mouse Ly-6C	HK1.4	
FITC-anti-mouse Ly-6G	1A8	
APC-anti-mouse PD-1	RMP1-30	
PE-anti-mouse TNF-α	MP6-XT22	
APC-anti-human CD3	HIT3a	
APC-anti-mouse CD11c PE-anti-mouse CD11c	N418	eBioscience
FITC-anti-mouse CD14	Sa2-8	
AlxaFluor700-anti-mouse CD45.2	104	
APC-anti-human CD3	HIT3a	
APC-anti-mouse CD11c PE-anti-mouse CD11c	N418	eBioscience
FITC-anti-mouse CD14	Sa2-8	
AlxaFluor700-anti-mouse CD45.2	104	
APC-anti-mouse NK1.1	PK136	
PE-anti-mouse PD-L1	MIH5	
FITC-anti-human CD8	T8	BECKMAN COULTER
ViaProbe (PerCP/Cy5.5-7AAD)		BD Bioscience

Table S2. Primers used for qPCR. Related to Figure 3, 4, S4.

Gene	Primer sequences	
	Forward	**Reverse**
Gapdh	5’-GCCTGGAGAAACCTGCCA-3’	5’-CCCTCAGATGCCTGCTTCA-3’
Gzmb	5’-TCCTGCTACTGCTGACCTTGTC-3’	5’-ATGATCTCCCCTGCCTTTGTC-3’
Ifng	5’-GATATCTGGAGGAACTGGCAAAAG-3’	5’-AGAGATAATCTGGCTCTGCAGGAT-3’
Prf1	5’-CAAGGTAGCCAATTTTGCAGC-3’	5’-GGCGAAAACTGTACATGCGAC-3’
Cxcl9	5’-GATAAGGAATGCACGATGCTC-3’	5’-TCTCCGTTCTTCAGTGTAGCAA-3’
Cxcl10	5’-GTGTTGAGATCATTGCCACGA-3’	5’-GCGTGGCTTCACTCCAGTTAA-3’
Cxcl11	5’-GGCTGCGACAAAGTTGAAGTGA-3’	5’-TCCTGGCACAGAGTTCTTATTGGAG-3’
Tbx21	5’-CAACCAGCACCAGACAGAGA-3’	5’-CCACATCCACAAACATCCTG-3’
Il12b	5’-AATGTCTGCGTGCAAGCTCA-3’	5’-ATGCCCACTTGCTGCATGA-3’